





# Methylotrophic methanogenesis in the *Archaeoglobi* revealed by cultivation of *Ca. Methanoglobus hypatiae* from a Yellowstone hot spring

Mackenzie M. Lynes <sup>1</sup>, Zackary J. Jay <sup>1</sup>, Anthony J. Kohtz <sup>1</sup>, Roland Hatzenpichler <sup>1,2,\*</sup>

<sup>1</sup>Department of Chemistry and Biochemistry, Center for Biofilm Engineering, Thermal Biology Institute, Montana State University, Bozeman, MT 59717, United States

<sup>2</sup>Department of Microbiology and Cell Biology, Montana State University, Bozeman, MT 59717, United States

\*Corresponding author: Roland Hatzenpichler, Department of Chemistry and Biochemistry, Montana State University, 111 Chemistry and Biochemistry Building, Bozeman, MT-59718, United States. Email: roland.hatzenpichler@montana.edu

## Abstract

Over the past decade, environmental metagenomics and polymerase chain reaction-based marker gene surveys have revealed that several lineages beyond just a few well-established groups within the *Euryarchaeota* superphylum harbor the genetic potential for methanogenesis. One of these groups are the *Archaeoglobi*, a class of thermophilic *Euryarchaeota* that have long been considered to live non-methanogenic lifestyles. Here, we enriched *Candidatus Methanoglobus hypatiae*, a methanogen affiliated with the family *Archaeoglobaceae*, from a hot spring in Yellowstone National Park. The enrichment is sediment-free, grows at 64–70°C and a pH of 7.8, and produces methane from mono-, di-, and tri-methylamine. *Ca. M. hypatiae* is represented by a 1.62 Mb metagenome-assembled genome with an estimated completeness of 100% and accounts for up to 67% of cells in the culture according to fluorescence *in situ* hybridization. Via genome-resolved metatranscriptomics and stable isotope tracing, we demonstrate that *Ca. M. hypatiae* expresses methylotrophic methanogenesis and energy-conserving pathways for reducing monomethylamine to methane. The detection of *Archaeoglobi* populations related to *Ca. M. hypatiae* in 36 geochemically diverse geothermal sites within Yellowstone National Park, as revealed through the examination of previously published gene amplicon datasets, implies a previously underestimated contribution to anaerobic carbon cycling in extreme ecosystems.

**Keywords:** archaea, MCR, methane, stable isotope tracing, thermophile, transcriptomics

## Introduction

Methanogenesis is one of the most ancient metabolic pathways and plays a major role in the biogeochemical carbon cycle. Phylogenomic reconstructions and geological evidence suggest that methanogenesis was among the earliest metabolisms to evolve and that the last common ancestor of all extant archaea likely was a methanogen [1–9]. Therefore, the study of methanogens is essential for understanding the co-evolution of life and the biosphere. Methanogenic archaea are the primary producers of biogenic methane (CH<sub>4</sub>) and contribute ~60% to the estimated 576 Tg of annual global methane emissions to the atmosphere [10, 11]. Methanogenic pathways are classified by their carbon and electron sources [12–14]. All methanogenic pathways converge at the terminal methane-forming step catalyzed by the methyl-coenzyme M reductase (MCR) complex. MCR and its homologs also catalyze the reverse reaction in the anaerobic oxidation of alkanes in alkanotrophic archaea [15, 16]. MCR is uniquely present in all methanogens and is commonly used to identify potential methane and/or alkane cycling archaea in sequencing surveys [12, 17].

The physiology and biochemistry of methanogens have near-exclusively been investigated in axenic cultures of

microorganisms belonging to the *Euryarchaeota* superphylum [12, 17–19]. These predominantly grow by acetoclastic or CO<sub>2</sub>-reducing hydrogenotrophic methanogenesis, with only rare observations of *Euryarchaeotal* methyl-reducing methanogens [12, 20, 21]. As a result, despite the dominance of methyl-based methanogenesis in anoxic environments with high salt and/or high sulfate concentration (e.g. anoxic marine sediments, coastal wetlands, hypersaline lakes), methylotrophic methanogenesis has in the past often been considered to be of comparatively limited environmental distribution. The extensive use of environmental metagenomics has led to the discovery of metagenome-assembled genomes (MAGs) encoding MCR from new lineages that are prevalent in anoxic environments, both within and outside the *Euryarchaeota* [2, 12, 22–26].

The majority of MAGs affiliated with archaeal phyla outside the *Euryarchaeota* are predicted to be methyl-reducing methanogens, with the exception of *Candidatus* (*Ca.*) *Nezhaarchaeota* [25, 27] and *Ca. Methanomixophus* affiliated with the order *Archaeoglobales*, which have been hypothesized to be CO<sub>2</sub>-reducing hydrogenotrophic methanogens [12, 25, 28]. This result is consistent with the observation that methylated methanogenic substrates, including methylamines and methanol, are prevalent in the environment, although their concentrations

Received 13 November 2023. Revised: 9 January 2024. Accepted: 8 February 2024.

© The Author(s) 2024. Published by Oxford University Press on behalf of the International Society for Microbial Ecology.

This is an Open Access article distributed under the terms of the Creative Commons Attribution License (<https://creativecommons.org/licenses/by/4.0/>), which permits unrestricted reuse, distribution, and reproduction in any medium, provided the original work is properly cited.

in hot springs is currently unknown. Furthermore, methyl-reducing methanogenesis is considered the predominant mode of methanogenesis in anoxic marine, freshwater, and hypersaline sediments (reviewed in Bueno de Mesquita et al. [20]).

Members of the class *Archaeoglobi* have long been considered non-methanogenic with isolates characterized as dissimilatory sulfate reducers brought into culture as early as 1987 [29]. To date, only nine species of the class *Archaeoglobi* have been obtained in axenic culture, and all were sourced from marine hydrothermal systems or off-shore oil reservoirs [30]. The discovery of both MCR [25, 31, 32] and methyl-H<sub>4</sub>M(S)PT:coenzyme M methyltransferase (MTR) complexes in genomes of the *Archaeoglobaceae* has suggested that members of this family may live by methanogenesis [28].

Very recently, important progress toward experimental verification of methanogenesis by members of this family has been made. Liu et al. reported the *in situ* expression of genes related to hydrogen-dependent methylotrophic methanogenesis and heterotrophic fermentation within populations of *Archaeoglobi* in a high-temperature oil reservoir [28]. Lynes et al. reported that *Archaeoglobi* can be enriched in hot spring mesocosms under methanogenic conditions [33]. Wang et al. reported that *mcrABG* and other methanogenesis marker genes encoded by two *Archaeoglobales* MAGs were highly expressed in hot spring microcosms incubated at 65°C and 75°C [34]. Importantly, one of these *Archaeoglobales* MAGs represented the only Mcr-encoding archaeon that expressed *mcrABG* genes in methanogenic microcosms performed without substrate addition or with the addition of 10 mM methanol at 75°C. This indirectly demonstrated the methanogenic nature of this archaeon [34]. Last, Buessecker et al. reported the establishment of a methanogenic enrichment culture of *Ca. Methanoglobus nevadensis* from Great Boiling Spring (GBS) (NV, USA) [35]. The culture yields up to 158 μM methane after 2 weeks of incubation at its optimal growth temperature of 75°C. *Ca. M. nevadensis* is represented by a 63% complete MAG obtained from the culture and a 98% complete MAG obtained a decade earlier [35].

Here, we report on the enrichment cultivation of *Ca. Methanoglobus hypatiae* LCB24, a methanogen affiliated with the family *Archaeoglobaceae*, from a hot spring in Yellowstone National Park (YNP). Using a combination of targeted cultivation, growth experiments, microscopy, stable isotope tracing, metagenomics, and metatranscriptomics, we demonstrate that *Ca. M. hypatiae* lives by methylotrophic methanogenesis and converts different methylamines to methane. By examining previously published datasets for the presence of Mcr-encoding *Archaeoglobi*, we demonstrate that these archaea are distributed in geothermal features of YNP, where they likely contribute to anaerobic carbon cycling. Our study presents direct evidence of methanogenesis within the *Archaeoglobaceae* and adds to the growing body of evidence demonstrating that methanogenesis is widely spread within the *Euryarchaeota* superphylum.

## Materials and Methods

All chemicals used in this study were sourced from Sigma Aldrich unless otherwise specified.

### Sample collection, enrichment, and cultivation

In November 2021, a slurry of sediment and water (1:9) was collected from an unnamed hot spring in the Lower Culex Basin of YNP, WY, USA. In our previous survey of Mcr-encoding archaea in YNP [33], this hot spring was given the identifier LCB024

(44.573294, -110.795388; pH 7.8, 67°C). A mixture of surface sediment (~1–2 cm deep) and hot spring water was collected into a glass bottle and sealed headspace-free with a thick butyl rubber stopper. Collected material was transported back to the lab and stored at room temperature. Using this material as inoculum, 30 ml enrichments were established in February 2022 in 60 ml serum bottles. Material was homogenized by mixing and was then diluted 1:10 (v/v) with anoxic medium in an anoxic glove box (N<sub>2</sub>/CO<sub>2</sub>/H<sub>2</sub>; 90/5/5%).

Medium was prepared anoxically as described previously [36]. Basal mineral medium contained a base of (per liter): KH<sub>2</sub>PO<sub>4</sub>, 0.5 g; MgSO<sub>4</sub>·7H<sub>2</sub>O, 0.4 g; NaCl, 0.5 g; NH<sub>4</sub>Cl, 0.4 g; CaCl<sub>2</sub>·2H<sub>2</sub>O, 0.05 g; HEPES, 2.38 g; yeast extract, 0.1 g; and 0.002% (w/v) (NH<sub>4</sub>)<sub>2</sub>Fe(SO<sub>4</sub>)<sub>2</sub>·6H<sub>2</sub>O. Medium was transferred to a Duran flask with a side opening and autoclaved for 20 m at 121°C. Medium was then further supplemented with 5 mM NaHCO<sub>3</sub>, 1 ml trace element solution SL-10, 1 ml Selenite-Tungstate solution, 1 ml CCM vitamins [37], 0.0005% (w/v) resazurin, 10 mg of coenzyme-M, 2 mg sodium dithionite, 1 mM dithiothreitol, 1 mM Na<sub>2</sub>S·9H<sub>2</sub>O, with pH adjusted to 7.8 using sodium hydroxide (NaOH, 12 N). Serum bottles were sealed with butyl rubber stoppers and aluminum crimps before the headspace were exchanged with N<sub>2</sub> (99.999%) for 5 min and set to a 200 kPa N<sub>2</sub> atmosphere. Monomethylamine (MMA) was added from a filter-sterilized methylamine-hydrochloride anoxic stock solution to a final concentration of 10 mM. The bacterial antibiotics streptomycin (50 mg/L; inhibitor of protein synthesis) and vancomycin (50 mg/L; inhibitor of peptidoglycan synthesis) were added from filter-sterilized anoxic stock solutions. The enrichments were incubated at 70°C in the dark without shaking. Cultures were maintained by regular transfer of 10% v/v into fresh media, which contained MMA and antibiotics. A sediment-free culture was obtained after the third transfer after which it was transferred at 10% v/v to 50 ml in 125 ml serum bottles.

### Stable isotope tracing

The conversion of <sup>13</sup>C- or D<sub>3</sub>-MMA (<sup>13</sup>CH<sub>3</sub>-NH<sub>2</sub>, CD<sub>3</sub>-NH<sub>2</sub>) to <sup>13</sup>CH<sub>4</sub> or CD<sub>3</sub>H was tracked by incubating active enrichment cultures in the presence of 20% labeled substrate (98%; Cambridge Isotope Laboratories). Incubations were carried out in 30 ml culture volumes in 60 ml serum bottles with 8% v/v inoculum, 50 mg/L streptomycin, 50 mg/L vancomycin, 10 mM MMA, and N<sub>2</sub> gas (99.999%) incubated in anoxic media (pH 7.8, 70°C) in six replicates (SI Appendix, Fig. S3). Duplicate control incubations included (i) <sup>12</sup>C-MMA and (ii) inoculum without MMA. Triplicate control incubations were performed with (iii) <sup>12</sup>C-MMA plus 10 mM bromoethanesulfonate (BES) added in mid-exponential phase (Day 33) to inhibit methanogenesis and (iv) 10 mM BES added at time of inoculation (Day 0) without substrate. Headspace samples were collected throughout the experiment as described above and analyzed using a Shimadzu QP2020 NX GCMS equipped with a GS-CarbonPLOT column (30 m × 0.35 mm; 1.5 μm film thickness; Agilent) and operated in Selected Ion Monitoring mode. The instrument was operated using the method described in Ai et al. [38] with helium as a carrier gas. All injections were performed by a Shimadzu AOC-6000 autosampler robot. Peak areas corresponding to m/z ratios of 16 for <sup>12</sup>CH<sub>4</sub>, 17 for <sup>13</sup>CH<sub>4</sub>, and 19 for CD<sub>3</sub>H were used for quantification.

### Metagenomic sequencing, assembly, and annotation

Two metagenomes were obtained over the course of this study. A 42 ml aliquot of the fourth transfer of the enrichment (Fig. 1

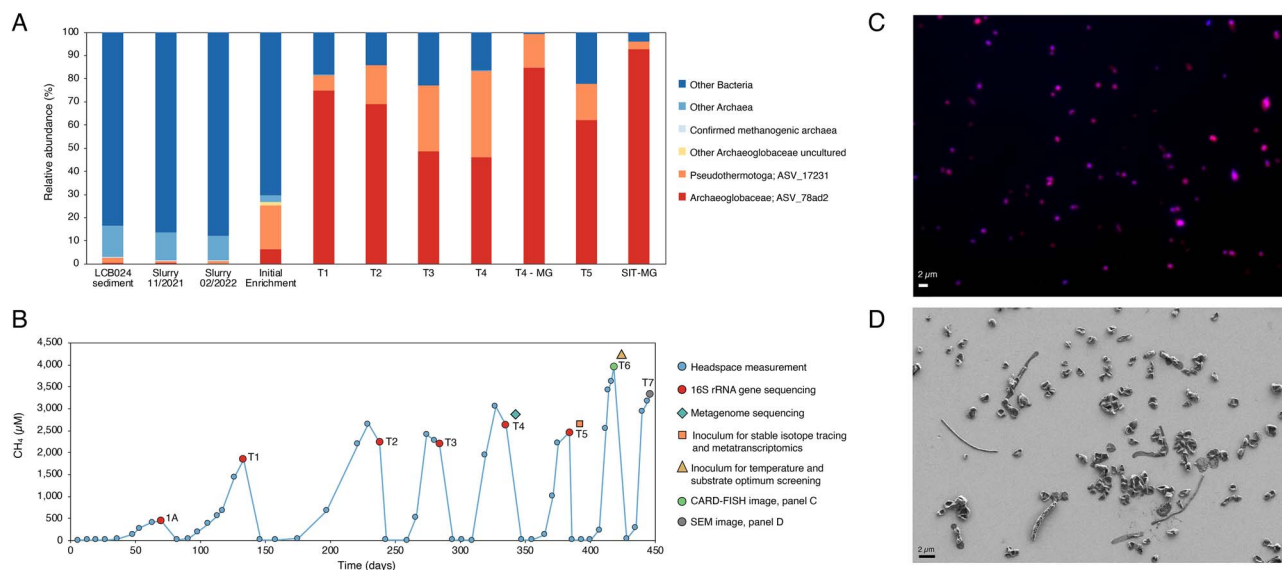


**Figure 1.** Community composition and methane production of the methanogenic enrichment culture containing *Ca. M. hypatiae* LCB24; (A) relative abundance of 16S rRNA gene amplicons in the initial sediment from hot spring LCB024, the slurry collected in November 2021, slurry material used to initiate enrichments in February 2022, the initial enrichment, and five subsequent transfers (T1–T5) are shown; for comparison, the estimated relative abundance of two metagenomic samples (T4-MG and SIT-MG) is included; the metagenome recovered from a replicate from the stable isotope tracing experiment incubated in the presence of deuterated methylamine (SIT-MG) revealed *Ca. M. hypatiae* grew to 92.8% relative abundance during the experiment; the two most abundant ASVs across enrichment transfers are shown with other taxa collapsed; other methanogenic archaea were not identified in the initial enrichment or in any subsequent transfer; relative sequence abundance for all ASVs is reported in [SI Appendix, Table S1](#); (B) headspace methane produced over long-term cultivation; the time between transfers decreased while the average maximum concentration of methane increased over time; culture 1A represents the initial enrichment; a history of methane measurements can be found in [SI Appendix, Table S2](#); (C) visualization of *Ca. M. hypatiae* cells at T6 labeled via CARD-FISH by the general archaea probe Arch915 (red). DAPI staining of cells is in blue; (D) cell morphologies in enrichment culture LCB24 at T7 as observed by SEM.

T4-MG) was filtered onto a 0.22 µm filter. The filter was transferred to a lysing matrix E tube and DNA extracted immediately following filtration. Genomic DNA was extracted using the FastDNA Spin Kit for Soil (MP Biomedicals, Irvine, CA) following the manufacturer’s guidelines.

A second metagenome was recovered from one of the six culture replicates grown in the presence of CD<sub>3</sub>-NH<sub>2</sub> and used for recruiting transcriptomic reads from the other replicates (Fig. 1 SIT-MG). A 60 ml syringe flushed with N<sub>2</sub> gas was used to transfer 30 ml of culture to a sterilized oak ridge tube. Cells were harvested through centrifugation for 30 min at 10000 rpm at 4°C. The supernatant was removed, and DNA extracted from the pellet using the FastDNA Spin Kit for Soil (MP Biomedicals, Irvine, CA) following the manufacturer’s guidelines. Genomic DNA for both metagenomes was shipped to SeqCenter (Pittsburgh, PA), and sample libraries were prepared using the Illumina DNA Prep kit and 10 bp unique dual indices (UDIs). The first metagenome (T4-MG) was sequenced on a NextSeq 2000 System (Illumina) and the second (SIT-MG) sequenced on a NovaSeq 6000 System (Illumina), each producing 2 × 151 bp reads. Demultiplexing, quality control, and adapter trimming were performed with bcl-convert v3.9.3. The quality of the reads was evaluated with FastQC before quality, linker and adapter trimming, artifact and common contaminant removal, and error correction were performed with the rqfilter2 pipeline (maxn = 3, maq = 10, trimq = 20) and bbcmcs (mincount = 2, hcf = 0.6). Resulting reads were assembled with SPAdes v3.15.13 (Nurk, 2017) (–k 33,55,77,99 127 –meta –only-assembler), and coverage was determined with bmap v38.94 (ambiguous = random) (<https://sourceforge.net/projects/bbmap>) [39]. In addition to the initial assembly, co-assemblies using both T4-MG and SIT-MG metagenomes were also performed [1] with reads directly fed into SPAdes with the –only-assembler option

excluded; and [2] with the trimmed and error corrected reads and the same SPAdes parameters as above. The statistics of MAGs generated through various assembly and quality control methods were evaluated, and the approach that produced the highest quality MAG was chosen for subsequent analysis (Dataset S1). The quality was determined by considering factors such as the number of resulting sequences, total length, completeness, and the minimum, maximum, and average sequence lengths. Annotation of the assembled sequences was performed with Prokka v1.14.16 [40]. Assembled scaffolds ≥2000 bp were binned using Maxbin v2.2.7 [41], Metabat v2.12.1 (with and without coverage) [42], Concoct v1.0.0 [43], Autometa v1 (bacterial and archaeal modes with the machine learning step) [44], followed by bin refinement with DAS\_Tool v1.1.6 [45], as previously described [46]. Bin completeness and redundancy were assessed with CheckM v1.2.2 [47].

### RNA extraction, sequencing, and transcriptomic processing

Total RNA was extracted for transcriptomics from four of the six replicates of *Archaeoglobus* cultivated in the presence of labeled substrate (<sup>13</sup>CH<sub>3</sub>-NH<sub>2</sub> or CD<sub>3</sub>-NH<sub>2</sub>) for a total of eight replicates. Each replicate culture in the exponential growth phase (Day 32) was moved from the 70°C incubator to an ice bath placed at –20°C for 40 mins to stop cellular activity. A 60 ml syringe flushed with N<sub>2</sub> gas was used to transfer 30 ml of culture to a sterilized oak ridge tube and kept on ice. Cells were harvested through centrifugation for 30 min at 10000 rpm at 4°C. The supernatant was removed, and the pellet transferred to a lysing matrix E tube (MP Biomedicals, Irvine, CA) to which 600 µL of RNA lysis buffer was added. Samples were homogenized in a MP Bioscience FastPrep instrument for 40 s at a speed setting

of 6.0 m/s followed by centrifugation for 15 min at 14000 rpm. RNA was extracted using the Quick-RNA miniprep kit (Zymo Research, Irvine, CA) including a DNase treatment step and eluted in 50  $\mu$ L of RNase free water. Centrifugation steps were performed at 15000 rpm and the final spin for elution at 10000 rpm. Of the eight replicates extracted, six measured  $>50$  ng/ $\mu$ L ( $3 \times$   $^{13}\text{CH}_3\text{-NH}_2$  and  $3 \times$   $\text{CD}_3\text{-NH}_2$ ) and were sent for transcriptomic sequencing at SeqCenter (Pittsburgh, PA). Samples were DNase treated with Invitrogen DNase (RNase free). Library preparation was performed using Illumina's Stranded Total RNA Prep Ligation with Ribo-Zero Plus kit and 10 bp UDI. Sequencing was done on a NovaSeq 6000, producing paired end 151 bp reads. Demultiplexing, quality control, and adapter trimming were performed with bcl-convert (v4.1.5). Read quality was further evaluated with FastQC v0.11.9 [48] before quality trimming and artifact, rRNA, and common contaminant removal with the rqcfilter2 pipeline (trimq=28, maxns=3, maq=20), and error correction with bbcm (mincount=2, hcf=0.6) from the BBTools suite v38.94 [39]. Additional rRNA gene reads were detected and removed with Ribodetector v0.2.7 [49], and any remaining rRNA gene reads were finally removed with bbmap, using rRNA genes recovered from the metagenomes (see below) as references. The resulting mRNA reads were mapped against annotated genes from the paired metagenomes with bbmap to calculate reads per kilobase of transcript per million mapped read (RPKM) (ambig=random).

## Results and Discussion

### Cultivation

In our recent survey on the diversity of Mcr-encoding archaea in the geothermal features of YNP, mesocosms seeded with biomass from a hot spring located within the Lower Culex Basin (LCB024; pH 7–8, 56–74°C) had shown potential to enrich for methanogenic *Archaeoglobi* [33]. Using a sediment slurry collected from LCB024, we initiated incubations supplied with MMA and antibiotics incubated in anoxic media (pH 7.8, 70°C) under a  $\text{N}_2$  headspace. The relative abundance, as determined by 16S rRNA gene amplicon sequencing, of *Archaeoglobi*-affiliated organisms in LCB024 was 0.32% in the initial slurry and had fallen to 0.02% by the time incubations were initiated a few months after samples had been collected (Fig. 1A).

Methane was detected after 36 days in the initial enrichment, and the culture was transferred to fresh media after reaching the late exponential phase of methane production following 70 days of incubation (447  $\mu\text{M}$ ; Fig. 1B). Five *Archaeoglobi*-related 16S rRNA gene amplicon ASVs were identified in the initial enrichment; however, one ASV grew to dominate the microbial community after the first transfer and reached 74.8% relative abundance after 62 days. In the transfers that followed, *Archaeoglobi*-related sequences became the only archaeal reads detected by 16S rRNA gene amplicon sequencing with the second most abundant organism a bacterium affiliated with the *Pseudothermotoga* at 6.8%. Although the  $\text{CO}_2$ -reducing methanogen *Methanothermobacter* sp. was detected at 0.45% relative abundance in the slurry material used for inoculation, it was not detected in any subsequent transfers, nor were any known methanogens. Over subsequent transfers (238 days, T2–T5), the relative abundance of *Archaeoglobi* ASVs ranged from 46% to 69%, and the final methane yield steadily increased from 1844 to 2459  $\mu\text{M}$ . A sediment-free enrichment was obtained by the third transfer. Starting with the fourth transfer, the culture volume was scaled from 30 ml to 50 ml. By the sixth transfer, the culture produced 3943  $\mu\text{M}$  methane within 34 days. Metagenomic sequencing at two timepoints (Day 335 of

the enrichment and Day 33 of the isotope tracing experiment described below) and 16S rRNA gene amplicon sequencing over recurring transfers (Fig. 1A) demonstrated that ASVs and MAGs affiliated with *Archaeoglobi* represented the only archaeon in culture LCB24. A single MCR complex (*mcrAGCDB*) belonging to the *Archaeoglobi* MAG was present, indicating this MAG represents the only methanogenic population.

### Metagenomics and phylogenetics

The reconstructed Mcr-encoding *Archaeoglobi* MAG from culture LCB24 was 1.62 Mbp in length with an estimated completeness of 100% according to checkM (SI Appendix, Table S3). This MAG was the result of a combined assembly of the T4-MG and SIT-MG metagenomes as this method yielded an improved assembly. Therefore, it was used for phylogenomic analysis against *Archaeoglobi* reference MAGs and genomes using 33 conserved single copy marker proteins and 16S rRNA genes (Fig. 2A and B, SI Appendix, Table S4). The phylogenomic analysis showed that MAGs encoding MCR complexes clustered separately from those lacking *mcr* gene sequences. Consistently, 16S rRNA gene phylogeny supported this clustering with a pronounced separation of hot spring reference genomes and MAGs from current known isolates of *Archaeoglobi*, resulting in three main clusters: (i) those retrieved from North American hot springs (YNP and GBS), (ii) those originating from hot springs in China, and (iii) isolates, all of which were obtained from deep-sea marine hydrothermal systems (Fig. 2B).

LCB24 and closely related reference MAGs and isolate genomes exhibited a range of amino acid identities (AAI, 52.6%–98.6%; Fig. 2C). Altogether, the LCB24 MAG was found to be highly related to previously obtained *Archaeoglobi* MAGs encoding the MCR complex and only distantly related to other *Archaeoglobales* sp. (AAI, 58.9%–65%; average nucleotide identity (ANI), 70.3%–70.6%; 16S rRNA ANI, 91.6%–93.8%; SI Appendix Figs S1 and S2). Based on AAI, MAG LCB24 was most closely related to *Archaeoglobi* LCB024-003 MAG (AAI, 98.6%), which we had obtained from the same hot spring in a previous study [33]. The ANI and AAI values to the closest cultured methanogen, *Ca. Methanoglobus nevadensis* GBS, are 80.2% and 83.3%, respectively. Based on these results, we designate this archaeon *Ca. M. hypatiae* strain LCB24, named after the philosopher Hypatia of Alexandria (for a protologue, see the SI Appendix, Results and Discussion). The estimated relative abundance of *Ca. M. hypatiae* based on the SIT-MG was 92.8%. Other community members in the LCB24 culture with  $>1\%$  relative sequence abundance included members of the *Pseudothermotoga* (3.2%), *Desulfoviregula* (1.7%), and the family *Moorellaceae* (1.3%) (Fig. 1A, Dataset S1).

The only *mcrAGCDB* genes recovered from both metagenomes belong to the genome of *Ca. M. hypatiae*. Phylogenetic analysis of the single copy of *McrA* indicated its close relationship to *McrA* sequences found in members of the TACK superphylum (Fig. 2D). This contrasts with the placement of *Ca. M. hypatiae* within the *Euryarchaeota* based on phylogenomics (Fig. 2A), suggesting that *Archaeoglobi* could have obtained the MCR complex as a result of a horizontal gene transfer event from an archaeon in the TACK superphylum [7, 8]. Also, it could indicate that non-methanogenic *Archaeoglobi* lost the capacity for anaerobic methane cycling after they had diverged from a shared methanogenic ancestor.

### Methanogenic activity of *Ca. M. hypatiae*

To gain insight into the activity of *Ca. M. hypatiae* under methanogenic and non-methanogenic conditions, a stable isotope tracing (SIT) experiment was conducted. Cultures were incubated

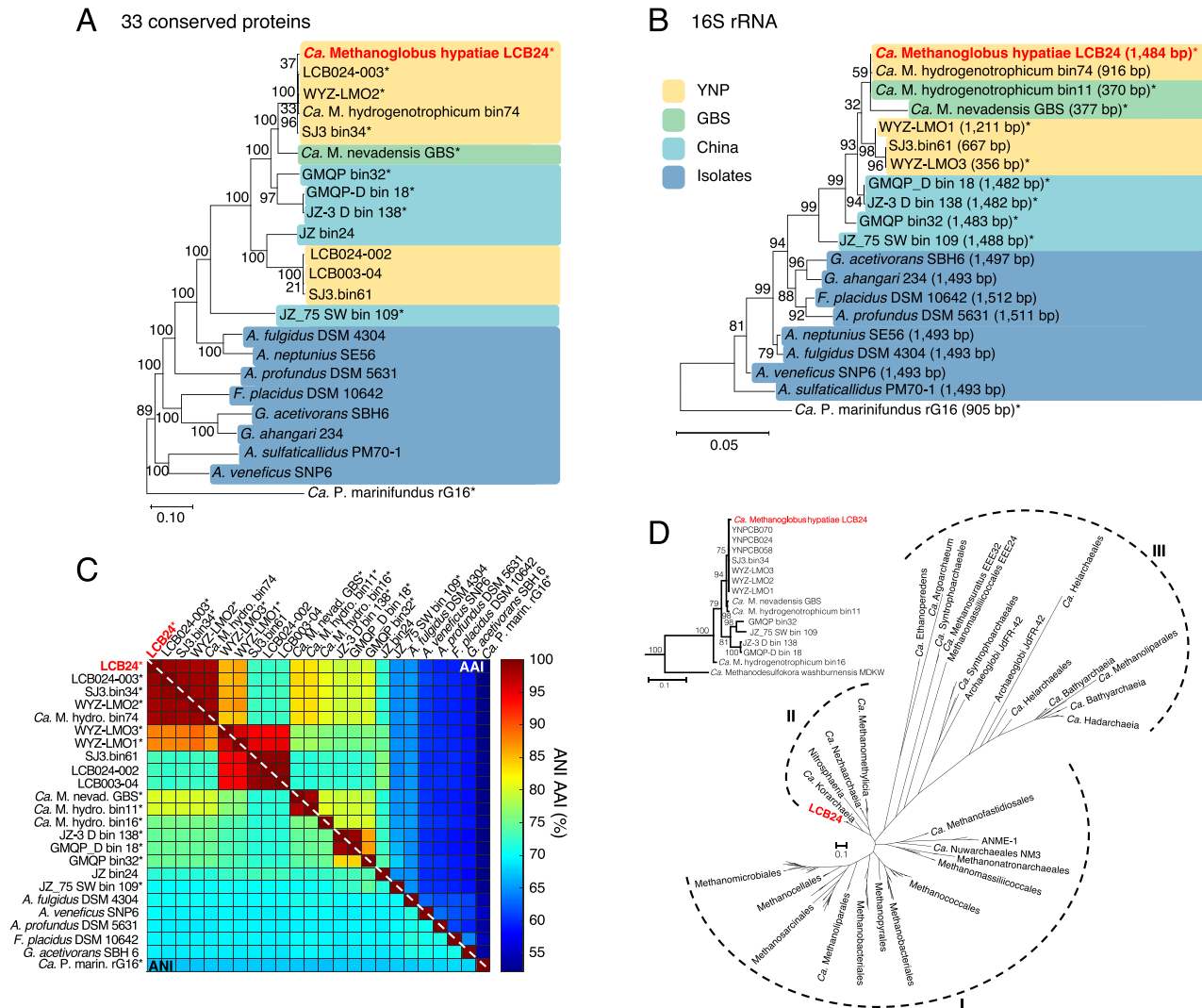


**Figure 2.** Phylogenetic affiliation of *Ca. M. hyptiae* LCB24; (A) maximum-likelihood tree, inferred with fasttree and WAG model (midpoint root), using a concatenated alignment of 33 conserved single copy proteins (list provided in SI Appendix, Table S4); references are colored by the habitat or type from which sequences had been recovered: hot springs in YNP, yellow; GBS, green; hot springs in China, blue; isolates from marine hydrothermal vent systems, dark blue; (B) maximum-likelihood tree inferred with fasttree using 16S rRNA genes with length in base pairs (bp); (C) ANI and AAI analysis of reference *Archaeoglobales* MAGs and genomes; asterisks (\*) indicate MAGs containing *mcrA*, apart from the MAG of *Ca. M. hydrogenotrophicum* bin74 which encodes a *mcrA* that is interrupted by a stop codon; AAI and ANI values are provided in SI Appendix, Fig. S1; (D) maximum-likelihood tree, inferred with IQtree2 and the LG + C60 + F + G model, from the amino acid alignment of *McrA*; dashed lines indicate *McrA/AcrA* groups: (I) *McrA* from methanogens and ANME (MCR-type), (II) *McrA* from TACK lineages (MCR-type), (III) *McrA*-like from proposed and experimentally confirmed alkane oxidizing archaea (ACR-type); insert shows MAGs closely related to *Ca. M. hyptiae* LCB24.

in the presence of 10 mM of MMA; 8 mM of substrate were isotopically light, whereas the remaining 2 mM consisted of either  $^{13}\text{C}$ -MMA ( $^{13}\text{CH}_3\text{-NH}_2$ ) or  $\text{D}_3$ -MMA ( $\text{CD}_3\text{-NH}_2$ ). Addition of the methanogenesis inhibitor BES was used as a non-methanogenic control (Figs 1B and 3, SI Appendix, Fig. S3). On average across six replicates, the cultured converted  $^{13}\text{CH}_3\text{-NH}_2$  to  $356 \mu\text{M } ^{13}\text{CH}_4$  (17.8%) and  $138.71 \mu\text{M } ^{13}\text{CO}_2$  (6.9%) by Day 32 (Fig. 3A and C, Dataset S2). The conversion of  $\text{CD}_3\text{-NH}_2$  was nearly identical yielding  $355 \mu\text{M } \text{CD}_3\text{H}$  (Fig. 3B). In the exponential phase of methane production, five of the six replicates were harvested for metagenomic and metatranscriptomic sequencing, while the sixth replicate was allowed to grow to stationary phase. The replicate allowed to grow in each respective experiment converted the provided  $^{13}\text{CH}_3\text{-NH}_2$  to  $717.7 \mu\text{M } ^{13}\text{CH}_4$  (35.9%) and  $212.95 \mu\text{M } ^{13}\text{CO}_2$  (10.65%) or  $\text{CD}_3\text{-NH}_2$  to  $394.76 \mu\text{M } \text{CD}_3\text{H}$  (19.7%) by Day 38 (Fig. 3A–C). These results confirmed that MMA was converted to methane by the LCB24 culture. The production of  $^{13}\text{CO}_2$  may

represent the dismutation of  $^{13}\text{CH}_3\text{-NH}_2$  to generate the reducing power for methanogenesis via the methyl-branch of the Wood–Ljungdahl pathway (WLP) or may be explained by other organisms in the culture catabolizing MMA. Yet, no transcriptomic evidence for this activity was present in this experiment. No methane production was observed for cultures treated with BES or in cultures incubated without MMA (Fig. 3D). When BES was added to cultures in the exponential phase, methane production ceased indicating the generation of methane is reliant on the *Archaeoglobi* MCR (Fig. 3E).

### Visualization and cell enumeration

The growth of *Ca. M. hyptiae* was tracked in four replicates during the SIT experiment with catalyzed reporter deposition fluorescence *in situ* hybridization (CARD-FISH) using a general archaea-targeted probe Arch915 [50] and DNA-staining (DAPI) (Fig. 1C). As the production of methane increased throughout the experiment,

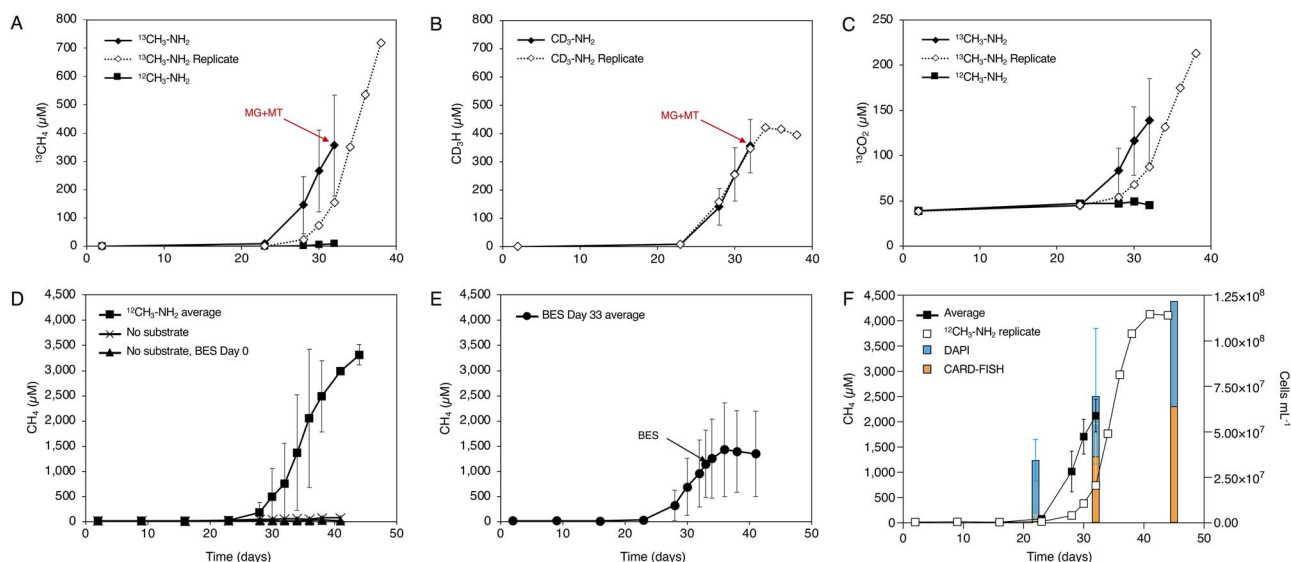


**Figure 3.** Conversion of stable isotope labeled MMA to methane by culture LCB24; (A) production of  $^{13}\text{CH}_4$  in cultures amended with  $^{13}\text{CH}_3\text{-NH}_2$  vs.  $^{12}\text{CH}_3\text{-NH}_2$  (six replicates); (B) production of  $\text{CD}_3\text{H}$  in cultures amended with  $\text{CD}_3\text{-NH}_2$  (six replicates); (C) production of  $^{13}\text{CO}_2$  in cultures amended with  $^{13}\text{CH}_3\text{-NH}_2$  vs.  $^{12}\text{CH}_3\text{-NH}_2$ ; for plots A and B, 10 total replicates across treatments were sacrificed during mid-exponential phase for metagenomic or metatranscriptomic sequencing indicated by red arrows;  $^{13}\text{CH}_4$ ,  $\text{CD}_3\text{H}$ , or  $^{13}\text{CO}_2$  production for the replicate allowed to reach stationary phase is shown as a dashed line through open diamond symbols; (D) production of  $^{12}\text{CH}_4$  in cultures amended with  $^{12}\text{C-MMA}$  ( $^{12}\text{CH}_3\text{-NH}_2$ ; 2 replicates); cultures incubated without substrates (two replicates) and those to which the inhibitor BES was added on Day 0 (3 replicates) did not produce  $^{12}\text{CH}_4$  over the course of the experiment; (E) production of  $^{12}\text{CH}_4$  in cultures amended with  $^{12}\text{CH}_3\text{-NH}_2$  to which BES was added on Day 33 of incubation (black arrow; three replicates); the average production of  $^{12}\text{CH}_4$  leveled off and ceased after the introduction of BES, indicating methane generation by *Ca. M. hypatiae* is MCR-dependent; error bars indicate standard deviation of biological replicates when applicable; measurements of  $^{12}\text{CH}_4$ ,  $^{13}\text{CH}_4$ ,  $\text{CD}_3\text{H}$ , and  $^{13}\text{CO}_2$  for all replicates and controls are reported in [Dataset S2](#);  $^{12}\text{CH}_4$  measurements for all controls and replicates are shown in [SI Appendix, Fig. S4](#) and [Dataset S3](#); (F)  $^{12}\text{CH}_4$  production and fraction of *Ca. M. hypatiae* cells in biological replicates incubated with  $^{13}\text{CH}_3\text{-NH}_2$ ; relative abundance of cells was determined at three time points (Days 22, 32, 45) based on the fraction of *Ca. M. hypatiae* specific CARD-FISH counts (orange) versus total counts of DAPI-stained cells (blue); error bars indicate the standard deviation for four biological replicates on Days 22 and 32.

there was a concurrent rise in the relative cell abundance of *Ca. M. hypatiae* (Fig. 3F, [SI Appendix, Table S5](#)). The initial assessment on Day 22 across four replicates revealed the total cell density to be  $3.45 \times 10^7 \pm 1.14 \times 10^7$  before substantial concentrations of methane had been detected in the headspace ( $<132 \mu\text{M}$ ). By Day 32, methane concentrations reached  $1777 \pm 739 \mu\text{M}$  and the total cell density increased to  $6.97 \times 10^7 \pm 3.73 \times 10^7$  cells  $\text{ml}^{-1}$  with 54% ( $\pm 9.6\%$ ) of cells labeled as *Ca. M. hypatiae* (Fig. 3F). All but one of these replicates were then sacrificed for further analysis. Finally on Day 45, the remaining replicate reached a headspace methane concentration of  $4109 \mu\text{M}$  and a total cell density of  $1.22 \times 10^8$  with 53% of cells labeled as *Ca. M. hypatiae*.

Visualization of the enrichment culture via scanning electron microscopy (SEM) revealed that most cells exhibited a regular to irregular coccoid morphology, with a width ranging from 0.5 to  $1 \mu\text{m}$  (Fig. 1D). This morphology has previously been described for other *Archaeoglobi* species [30, 51–53].

### Alternative substrates and temperature optimum

We determined the substrate and temperature range of *Ca. M. hypatiae* by growing the culture in the presence of several substrates at  $70^\circ\text{C}$  or with 10 mM MMA at  $60\text{--}85^\circ\text{C}$  (Fig. 4A and B). Conditions that lead to the production of methane included 10 mM trimethylamine (TMA), 10 mM dimethylamine (DMA), 10 mM MMA in media without yeast extract, and the control with 10 mM MMA and 0.01% yeast extract. Methane production of cultures grown with MMA in the presence or absence of yeast extract was indistinguishable ( $5202 \pm 606$  and  $5703 \pm 410 \mu\text{M}$   $\text{CH}_4$ , respectively) indicating that yeast extract is not essential for methanogenic growth. Observed methane concentrations were higher in incubations amended with DMA ( $10115 \pm 836 \mu\text{M}$

$\text{CH}_4$ ) and TMA ( $9524 \pm 3626 \mu\text{M}$   $\text{CH}_4$ , with a wide range of  $5361\text{--}11993 \mu\text{M}$ ) on average more than the MMA controls, consistent with what has been observed for other methylotrophic methanogens [54]. Incubations amended with 10 mM methanol (MeOH) did not produce methane after 47 days of incubation at  $70^\circ\text{C}$ . Due to its use by sulfate-reducing organisms as an electron donor [55], 10 mM lactate (LAC) was tested, as well as 10 mM MMA with 10 mM LAC, but none of these incubations produced methane. Production of methane has not been observed in any attempted transfers where hydrogen (99.9999% purity) was present in the headspace, or hydrogen with MMA was added.

The enrichment grew optimally at both  $64$  and  $70^\circ\text{C}$  with relative amounts of methane produced at  $5304 \pm 451 \mu\text{M}$  and  $5202 \pm 606 \mu\text{M}$ , respectively. This deviates from the predicted optimal growth temperature of  $74.4^\circ\text{C}$ , which was derived from the translation of proteins in the *Ca. M. hypatiae* MAG using Tome [56]. This is lower than the observed range of growth and optimum temperatures for type strains of non-methanogenic *Archaeoglobi* which have been demonstrated to grow between  $50$  and  $95^\circ\text{C}$  with optimal temperatures between  $75$  and  $83^\circ\text{C}$  in organisms sourced predominantly from deep sea vent environments [30]. No methane production was detected at temperatures  $77^\circ\text{C}$  or above or lower than  $64^\circ\text{C}$  after 47 days of incubation ([Dataset S4](#)).

### Genomic and transcriptomic basis for methanogenesis

The assembled metagenome obtained at the end of the SIT experiment was used to align a total of 23 376 154 metatranscriptome mRNA reads obtained from six replicates harvested in the exponential growth phase and to create a detailed reconstruction of the metabolism of *Ca. M. hypatiae* (Figs 3A and B and 5,

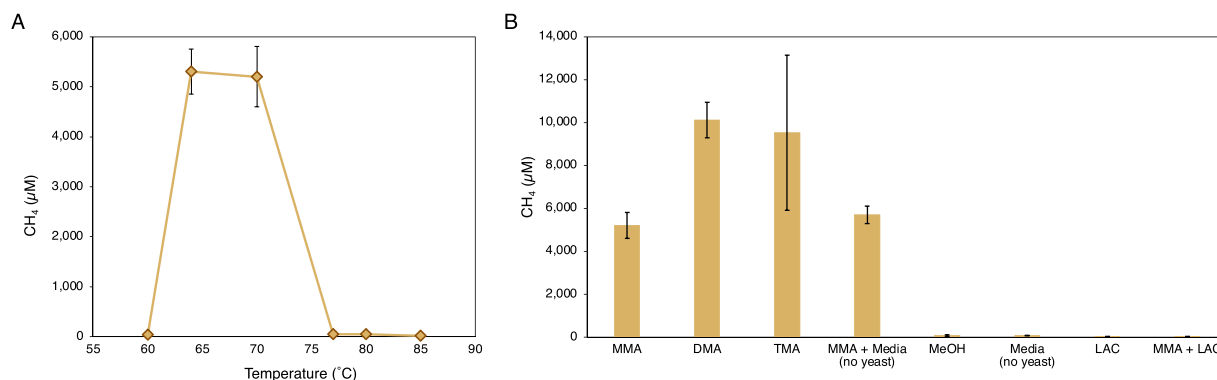


**Figure 4.** Temperature and substrate range of culture LCB24; (A) methane production from MMA was observed between 64 and 70°C; (B) substrate range; methane production was observed for MMA, DMA, TMA, and in media prepared without yeast extract; MeOH, methanol; both experiments performed in triplicate; all measurements can be found in [Dataset S4](#).

[Dataset S5](#)). A total of 22 891 651 reads, i.e. 97.8% of all recovered reads, were recruited to the *Ca. M. hypatiae* MAG. Only 2.1% of the total mRNA reads (484 503) were aligned with other co-enriched organisms. Among these, only 13 genes across four MAGs were expressed above 200 RPKMs and just five genes exceeded >1000 RPKM. Genes required for the conversion of methylamine to methane were among the top 2% of highest expressed genes transcribed by *Ca. M. hypatiae*, including genes encoding the MCR complex (*mcrAGCDB*; 13 046–18 098 RPKM), one of three MMA methyltransferase copies (*mtmB*; 9884 RPKM), DMA corrinoid (*mtbC*; 3677 RPKM), and methanol:coenzyme M methyltransferase (*mtaA*; 12 577 RPKM) (Fig. 5). Seven copies of substrate-specific methyltransferases for MMA (*mtmB*; 3 copies), DMA (*mtbB*; 2 copies), and TMA (*mttB*; 2 copies) were present in the genome, but methanol methyltransferase (*mtaB*) was not identified. These genes were differentially expressed with one copy for each type of methylamine expressed above 3200 RPKM. In addition to *mtbC*, two gene copies of the TMA corrinoid protein (*mttC*) were found in the genome but their expression was relatively low (<460 RPKM average). MMA corrinoid (*mtmC*) or methanol corrinoid (*mtaC*) proteins were not identified in *Ca. M. hypatiae*. Additionally, genes were expressed for pyrrolysine synthesis (*pylBCD*; 819, 343, 37 RPKM) and the methyltransferase corrinoid activation protein (*ramA*; 1076 RPKM), both of which support methylamine methyltransferases in methylotrophic methanogenesis [57, 58]. The absence of *mtmC* and the high expression levels of *mtbC* (3677 RPKM) and *mtaA* (12 577 RPKM) suggest that they are responsible for the transfer of a methyl group from MMA to coenzyme M (CoM) after it has been transferred by a substrate-specific methyltransferase (*mtmB*). Consistent with the observed methane production from DMA and TMA, *Ca. M. hypatiae* can use these methylamines and expressed the corresponding genes (*mtbB*, *mttB*) at comparatively high levels (JOOIALLP\_01813 *mtbB* 3249 RPKM; JOOIALLP\_01787 *mttB* 5324 RPKM; Figs 4B and 5). It is worth noting that the expression of *mtbB*/*mttB* was detected despite the culture not having been previously exposed to DMA or TMA at the time of the transcriptomics experiment. We hypothesize that *Ca. M. hypatiae* could employ one of two strategies: it either (i) constitutively expresses all substrate-specific methyltransferases and corrinoid proteins as a precautionary measure to accommodate substrates potentially encountered *in situ*, or (ii) *Ca. M. hypatiae* transcriptionally co-regulates the genes responsible for these functions.

*Ca. M. hypatiae* expressed the methyl-branch of the WLP and the acetyl-CoA decarboxylase/synthase complex (Cdh,

*cdhABCDE*), which is consistent with genes observed and shown to be expressed in sulfate-reducing *Archaeoglobi* genomes [55]. This includes two paralogous copies of 5,10-methylenetetrahydromethanopterin reductase (*mer*) which might function as a traditional Mer, considering that these genes are also members of the large luciferase-like monooxygenase family (pfam00296) [35]. The expression of genes in the WLP varied. Methylenetetrahydromethanopterin dehydrogenase (*mtd*), methenyltetrahydromethanopterin cyclohydrolase (*mch*), formylmethanofuran-tetrahydromethanopterin N-formyltransferase (*ptr*), formylmethanofuran dehydrogenase (*fwdABC*), and one copy of the *mer* homologs were expressed at comparatively high levels (456–2763 RPKM), whereas FwdDEFG and the other *mer* copy were only minimally expressed (<180 RPKM) (Dataset S5). The high expression of the Cdh complex (*cdhACDE*; 3063 ± 362, *cdhB* 677 RPKM average across subunits) suggests that *Ca. M. hypatiae* is capable of autotrophically fixing CO<sub>2</sub> to acetyl-CoA as has been shown for other *Archaeoglobus* species [59]. Acetyl-CoA could also be derived from the degradation of fatty acids present in yeast extract through the process of beta-oxidation. Enzymes involved in this pathway were expressed at moderate to high levels during growth (Dataset S6). Pyruvate synthase (Pps) was highly expressed providing a way for acetyl-CoA to be converted to pyruvate and subsequently be fed into major biosynthetic pathways. Specifically, *Ca. M. hypatiae* encodes pyruvate carboxylase (PycAB), an incomplete reductive tricarboxylic acid cycle (rTCA), phosphoenolpyruvate synthase (Pps), most enzymes needed for gluconeogenesis, and several enzymes associated with the pentose phosphate pathway in archaea, which were all expressed at varying levels (Dataset S5). Together, these pathways provide *Ca. M. hypatiae* the capacity to synthesize amino acids, carbohydrates, integral components of the cell wall, and vital sugars for nucleic acids.

Several complexes related to energy conservation and electron transport were moderately to highly expressed. *Ca. M. hypatiae* encodes a fused heterodisulfide reductase (*hdrDE*) that was highly expressed (1106 ± 120 RPKM) in addition to a fused *hdrD/mvhD* and four copies of *hdrD* that were all expressed at much lower levels (<500 RPKM). The differing levels of transcription suggest that the membrane-bound HdrDE is responsible for the regeneration of coenzymes M and B through the reduction of heterodisulfide (CoM-S-S-CoB). Additionally, the absence of HdrB, which contains the active site for disulfide reduction, eliminates the possibility that disulfide reduction could occur via a HdrABC complex [60]. As reported for *Ca. M. nevadensis* [35], a unique gene cluster was

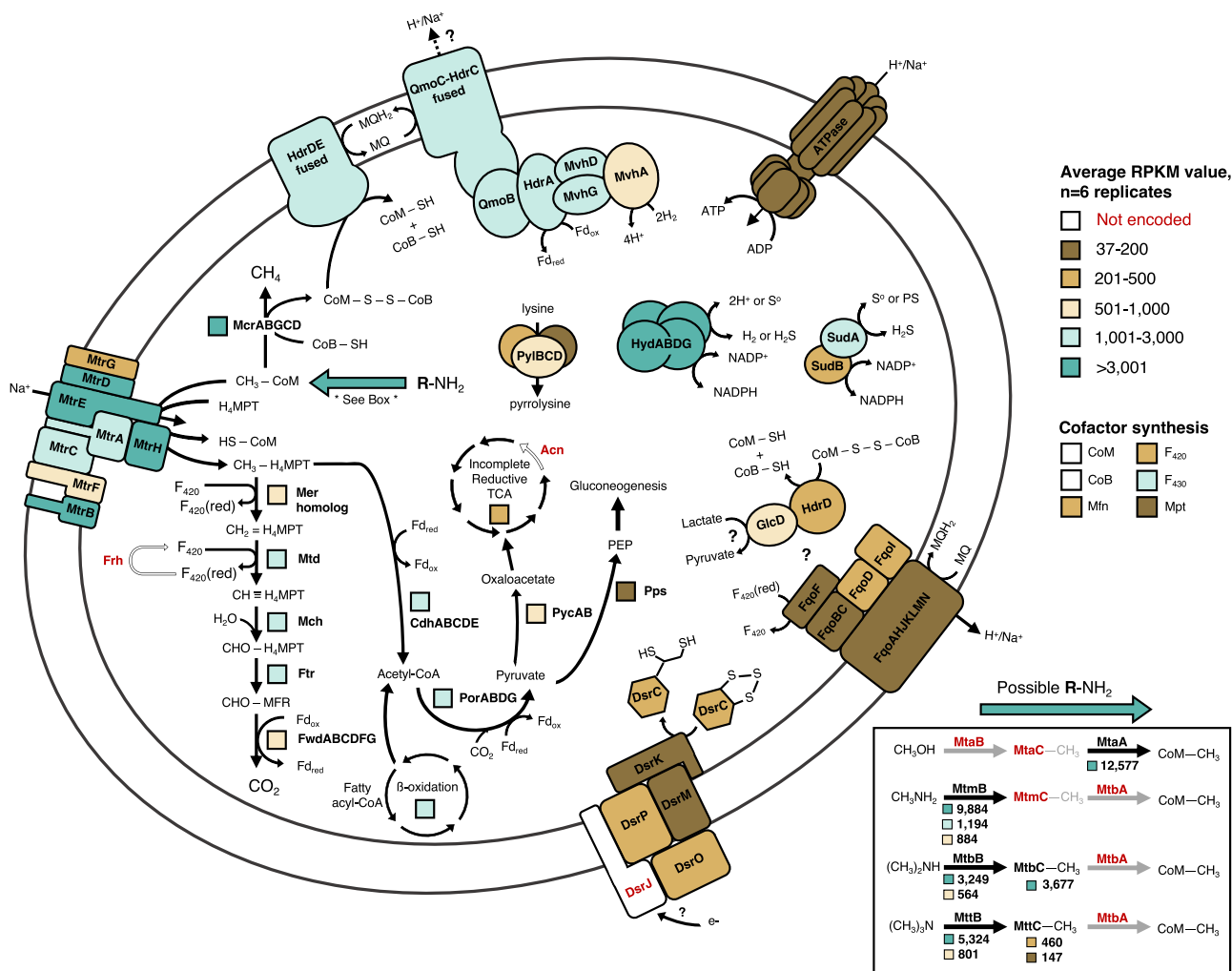


**Figure 5.** Transcriptional activity in *Ca. M. hypatiae* grown under methanogenic conditions (N<sub>2</sub> headspace, 10 mM MMA, and 0.01% yeast extract); transcriptionally active proteins are shown in bold black font; proteins not encoded in the MAG are colored in white and denoted in bold red font; average RPKMs values of six biological replicates are depicted; RPKM values are represented by boxes or colored subunits close to each protein and are colored according to their expression level with the RPKM value of the lowest expressed gene depicted, 37 RPKM; for enzymes comprising multiple subunits, the beta-oxidation pathway, and the TCA cycle, an average RPKM value representing the transcribed enzymes is used. *Ca. M. hypatiae* is transcriptionally active under methanogenic conditions and encodes the ability to convert methyl-groups from mono-, di-, and TMA to methane; this ability is enabled by several copies of substrate-specific methyltransferases and corrinoid proteins highlighted in the box to the bottom right; a complete list of genes described in this figure, their transcription levels, and their abbreviations is provided in [Dataset S5](#).

identified containing F<sub>420</sub>-non-reducing hydrogenase (MvhAGD), two HdrA copies and a QmoC fused to a HdrC. One HdrA copy (JOOIALLP\_01710) was predicted by DiSCO analysis as a quinone-modifying oxidoreductase (QmoB), a protein related to the HdrA of methanogens [61, 62]. This cluster was expressed at high levels (995–2431 RPKM average), suggesting its importance for electron transfer in *Ca. M. hypatiae*. We hypothesize that these subunits are associating together *in vivo* to bifurcate electrons from hydrogen (H<sub>2</sub>) to reduce both menaquinone (MQ) and ferredoxin (Fd<sub>ox</sub>), as proposed recently [35, 63]. Lastly, *Ca. M. hypatiae* moderately expressed a membrane-bound F<sub>420</sub>H<sub>2</sub>:quinone oxidoreductase (Fqo) complex (88–280 RPKM across subunits) and a V-type ATP synthase (24–442 RPKM across subunits).

The electrons required for reducing the CoM-S-S-CoB heterodisulfide could originate from two possible routes. The first possibility would rely on sourcing electrons from hydrogen, which could be oxidized by the Mvh-Qmo-Hdr complex coupled to MQ reduction. H<sub>2</sub> may be produced through the activity of a group 3b [NiFe]-sulfhydrogenase (HydABDG), which was the

highest expressed hydrogenase complex with an average RPKM of 4421 across subunits [64, 65]. To evolve hydrogen via HydABDG, reducing power, via NADPH, could be supplied by sulfide dehydrogenase (SudAB; SudA, 1088 RPKM; SudB, 495 RPKM). Alternatively, NADPH could instead be provided to biosynthesis pathways and therefore be decoupled from methanogenic metabolism. H<sub>2</sub> could also potentially be sourced from fermentative bacteria in the enrichment culture; however, the low number of hydrogenases encoded by co-enriched organisms was only very lowly expressed at the time of sampling for metatranscriptomics (<51 RPKM). At this point, the source of H<sub>2</sub> *Ca. M. hypatiae* uses remains uncertain, as no H<sub>2</sub> was added to the headspace. The second option for reducing the CoM-S-S-CoB heterodisulfide involves a hydrogen-independent electron transport system, where reduced F<sub>420</sub> and ferredoxin are generated through the dismutation of methylated substrate to CO<sub>2</sub> via the WLP. Reduced F<sub>420</sub> could be oxidized by the Fqo complex and contribute to a reduced MQ pool that could be used by the fused HdrDE complex to reduce CoM-S-S-CoB. Reduced ferredoxin could be oxidized at a soluble FqoF



to reduce  $F_{420}$  or at an F<sub>420</sub> complex lacking FqoF to reduce MQ [66, 67]. Based on the low expression levels of the F<sub>420</sub> complex ( $171 \pm 67$  RPKM) and the absence of  $F_{420}$ -reducing hydrogenase (*frh*) from the genome, it is not likely the WLP runs in the reductive direction as a source of reduced  $F_{420}$  would be required. Resolving the exact configuration of the electron transport system encoded by *Ca. M. hypatiae* will require biochemical confirmation in future investigations.

Genes necessary for dissimilatory sulfate reduction typically observed in sulfate-reducing members of the *Archaeoglobi*, including dissimilatory sulfite reductase (*dsrAB*), sulfate adenylyltransferase (*sat*), and adenylylsulfate reductase (*aprAB*), were neither identified in the genome of *Ca. M. hypatiae* nor in the unbinned fraction of the metagenome. They were also absent from the comparatively incomplete MAG of *Ca. M. nevadensis* GBS [35]. However, *Ca. M. hypatiae* encodes subunits *dsrMK* and *dsrOP* of the Dsr complex in addition to *dsrC*. This complex is strictly conserved in sulfate-reducing organisms [68] where it mediates electron transfer from the periplasm to the cytoplasm reducing the disulfide bond found in DsrC cysteines [69]. The expression of the Dsr complex and *dsrC* was low ( $450 \pm 63$  RPKM) during growth on MMA suggesting it is not vital to the metabolism of *Ca. M. hypatiae*. The presence of the Dsr complex, DsrC, and subunits QmoC and QmoB in the genome may be explained as evolutionary remnants from ancestral *Archaeoglobi*, growing initially as sulfate-reducing organisms but later transitioning to a methanogenic lifestyle [7, 8]. This raises the question whether intermediate of this process, *Archaeoglobi* capable of both methanogenesis and sulfate-reduction (and possible anaerobic oxidation of methane), still exist today [25, 28].

Collectively, the metagenomic and transcriptomic data confirmed that *Ca. M. hypatiae* is not only the sole archaeon but the sole methanogen in our culture. The metabolic reconstruction and metatranscriptomic results are consistent with methylotrophic methanogenesis from methylamines. The absence of genes required for sulfate reduction eliminates the possibility for this metabolism in *Ca. M. hypatiae*. A unique gene cluster (Mvh-Qmo-Hdr) potentially involved in energy conservation was expressed; however, future studies will be required to test how *Ca. M. hypatiae* internally cycles electrons for methanogenesis and if it sources  $H_2$ , or other reductants, from the medium or co-enriched bacteria.

### Distribution of *Ca. methanoglobus* across geothermal features in YNP

16S rRNA and *mcrA* gene amplicon sequence data generated in a recent microbial diversity survey of 100 geothermal features in YNP [33] were used to analyze the distribution of *Archaeoglobi* related to *Ca. M. hypatiae* (SI Appendix, Fig. S5). 16S rRNA gene amplicons closely related to *Ca. M. hypatiae* (96.7%–100% sequence identity) were found in seven DNA samples from six hot springs (pH 5.1–9.35, 31–78°C) in addition to hot spring LCB024 (the source of this culture) at relative abundances ranging from 0.02% to 0.22%. In addition, *mcrA* gene ASVs affiliated with *Archaeoglobi* were PCR-amplified from 53 DNA samples, out of 201 total samples that had been screened by PCR. These 53 samples had been collected from microbial mats or sediments originating from 36 geothermal features distributed across various thermal regions within YNP by Lynes et al. [33]. *Archaeoglobi*-related *mcrA* genes were found in geothermal features with a pH range of 2.61 to 9.32 and a temperature range of 18.4–93.8°C. Collectively, our results and the studies by Wang et al. and Buessecker et al., who reported that Mcr-encoding

*Archaeoglobi* are present [35] and transcriptionally active in hot spring mesocosms [34], demonstrate the previously overlooked role that *Archaeoglobi* might play in the anaerobic carbon cycle of geothermal environments.

## Conclusion

The cultivation of *Ca. M. hypatiae* LCB24 provides direct experimental evidence that members of the *Archaeoglobi* are methanogens. *Ca. M. hypatiae* can use MMA, DMA, and TMA as methanogenic substrates and grows optimally at 64–70°C, as evidenced by metagenomics, metatranscriptomics, and isotope tracing experiments. Metagenomic sequencing and phylogenomic analysis confirmed the close relationship of *Ca. M. hypatiae* to other Mcr-encoding *Archaeoglobi* and the relatedness of its *mcrA* to MAGs of the TACK superphylum, some of which have recently been shown to also be methanogens [70, 71]. Together, this supports the idea that the capacity for methanogenesis is deeply rooted in the archaea and possibly dates to the last common ancestor of archaea [1, 3, 7, 8, 72]. The wide distribution of *Archaeoglobi*-affiliated *mcrA* gene sequences and *Ca. M. hypatiae*-related 16S rRNA gene sequences in geothermal features across YNP suggests that members of this lineage play a hitherto unaccounted-for role in anaerobic carbon cycling in these extreme ecosystems. Future studies of *Ca. M. hypatiae* and other methanogens will provide valuable insights into the evolution of methane metabolism and the significance of these archaea in biogeochemical cycles across geothermal and other environments.

## Acknowledgements

We thank the US National Park Service for permitting work in YNP under permit number YELL-SCI-8010. We thank George Schaible (MSU) for the help with SEM imaging, Dr Viola Krukenberg (MSU) for initial FISH methodology development, Sylvia Nupp, Dr Andrew Montgomery, and Paige Schlegel (all MSU) for the assistance with field sampling, Dr Christopher Lemon (MSU) for allowing use of his cooling centrifuge, and Dr Marike Palmer (UN Las Vegas) for discussing naming of this archaeon.

## Author contributions

Mackenzie M. Lynes and Roland Hatzenpichler developed the research project. Mackenzie M. Lynes, Zackary J. Jay, Anthony J. Kohtz, and Roland Hatzenpichler designed experiments. Mackenzie M. Lynes and Anthony J. Kohtz conducted field sampling. Mackenzie M. Lynes performed cultivation, extracted DNA for amplicon and metagenomic sequencing, extracted RNA for transcriptomic sequencing, and conducted physiology and stable isotope experiments. Anthony J. Kohtz developed GC/GCMS protocols and processed GCMS samples. Zackary J. Jay processed and annotated metagenomic and transcriptomic data, assembled MAGs, mapped transcripts, assigned taxonomy, constructed 16S rRNA gene phylogeny, and performed phylogenetic analysis of MAGs. Mackenzie M. Lynes conducted phylogenetic analysis of amplicon data, refined gene annotations, reconstructed, and interpreted the metabolic potential of *Ca. M. hypatiae* with insight from Zackary J. Jay and Anthony J. Kohtz. Roland Hatzenpichler was responsible for funding and supervision of the project. Mackenzie M. Lynes and Roland Hatzenpichler wrote the manuscript, which was then edited by all authors.

## Supplementary material

Supplementary material is available at *The ISME Journal* online.

## Conflicts of interest

None declared.

## Funding

This study was funded through a NASA Exobiology program award (80NSSC19K1633) to R.H.

## Data availability

All metagenomic, metatranscriptomic, and amplicon data discussed in this manuscript are available under NCBI BioProject ID PRJNA1014417. McrA gene amplicon data from YNP hot springs discussed in this manuscript have been previously published (Lynes et al.) and are available under NCBI under BioProject PRJNA859922.

## References

- Wolfe JM, Fournier GP. Horizontal gene transfer constrains the timing of methanogen evolution. *Nat Ecol Evol* 2018;**2**:897–903. <https://doi.org/10.1038/s41559-018-0513-7>
- Sorokin DY, Makarova KS, Abbas B et al. Discovery of extremely halophilic, methyl-reducing euryarchaea provides insights into the evolutionary origin of methanogenesis. *Nat Microbiol* 2017;**2**:17081. <https://doi.org/10.1038/nmicrobiol.2017.81>
- Martin WF, Sousa FL. Early microbial evolution: the age of anaerobes. *CSH Perspect Biol* 2016;**8**:a018127. <https://doi.org/10.1101/cshperspect.a018127>
- Sauterey B, Charnay B, Affholder A et al. Co-evolution of primitive methane-cycling ecosystems and early Earth's atmosphere and climate. *Nat Commun* 2020;**11**:2705. <https://doi.org/10.1038/s41467-020-16374-7>
- Ueno Y, Yamada K, Yoshida N et al. Evidence from fluid inclusions for microbial methanogenesis in the early Archaeal era. *Nature* 2006;**440**:516–9. <https://doi.org/10.1038/nature04584>
- Spang A, Ettema TJG. Archaeal evolution: the methanogenic roots of Archaea. *Nat Microbiol* 2017;**2**:17109. <https://doi.org/10.1038/nmicrobiol.2017.109>
- Adam PS, Kolyfetis GE, Bornemann TLV et al. Genomic remnants of ancestral methanogenesis and hydrogenotrophy in Archaea drive anaerobic carbon cycling. *Sci Adv* 2022;**8**:eabm9651. <https://doi.org/10.1126/sciadv.abm9651>
- Wang Y, Wegener G, Williams TA et al. A methylotrophic origin of methanogenesis and early divergence of anaerobic multi-carbon alkane metabolism. *Sci Adv* 2021;**7**:eabj1453. <https://doi.org/10.1126/sciadv.abj1453>
- Hinrichs K-U. Microbial fixation of methane carbon at 2.7 Ga: was an anaerobic mechanism possible? *Geochem Geophys Geosy* 2002;**3**:1–10. <https://doi.org/10.1029/2001GC000286>
- Saunio M, Stavert AR, Poulter B et al. The global methane budget 2000–2017. *Earth Syst Sci Data* 2020;**12**:1561–623. <https://doi.org/10.5194/essd-12-1561-2020>
- Rosentreter JA, Borges AV, Deemer BR et al. Half of global methane emissions come from highly variable aquatic ecosystem sources. *Nat Geosci* 2021;**14**:225–30. <https://doi.org/10.1038/s41561-021-00715-2>
- Garcia PS, Gribaldo S, Borrel G. Diversity and evolution of methane-related pathways in archaea. *Annu Rev Microbiol* 2022;**76**:727–55. <https://doi.org/10.1146/annurev-micro-041020-024935>
- Ferry JG, Kestrad KA. Methanogenesis. In: Cavicchioli R. (ed.), *Archaea: Molecular and Cellular Biology*. ASM Press, 2007, 288–314.
- Conrad R. The global methane cycle: recent advances in understanding the microbial processes involved. *Env Microbiol Rep* 2009;**1**:285–92. <https://doi.org/10.1111/j.1758-2229.2009.00038.x>
- Scheller S, Goenrich M, Boecher R et al. The key nickel enzyme of methanogenesis catalyses the anaerobic oxidation of methane. *Nature* 2010;**465**:606–8. <https://doi.org/10.1038/nature09015>
- Thauer RK. Methyl (alkyl)-coenzyme M reductases: nickel F-430-containing enzymes involved in anaerobic methane formation and in anaerobic oxidation of methane or of short chain alkanes. *Biochemistry* 2019;**58**:5198–220. <https://doi.org/10.1021/acs.biochem.9b00164>
- Evans PN, Boyd JA, Leu AO et al. An evolving view of methane metabolism in the Archaea. *Nat Rev Microbiol* 2019;**17**:219–32. <https://doi.org/10.1038/s41579-018-0136-7>
- Thauer RK, Kaster AK, Seedorf H et al. Methanogenic archaea: ecologically relevant differences in energy conservation. *Nat Rev Microbiol* 2008;**6**:579–91. <https://doi.org/10.1038/nrmicro1931>
- Baker BJ, De Anda V, Seitz KW et al. Diversity, ecology and evolution of Archaea. *Nat Microbiol* 2020;**5**:887–900. <https://doi.org/10.1038/s41564-020-0715-z>
- Bueno de Mesquita CP, Wu D, Tringe SG. Methyl-based methanogenesis: an ecological and genomic review. *Microbiol Mol Biol Rev* 2023;**87**:e00024–2. <https://doi.org/10.1128/mmlr.00024-22>
- Söllinger A, Urich T. Methylotrophic methanogens everywhere — physiology and ecology of novel players in global methane cycling. *Biochem Soc Trans* 2019;**47**:1895–907. <https://doi.org/10.1042/BST20180565>
- Nobu MK, Narihito T, Kuroda K et al. Chasing the elusive *Euryarchaeota* class WSA2: genomes reveal a uniquely fastidious methyl-reducing methanogen. *ISME J* 2016;**10**:2478–87. <https://doi.org/10.1038/ismej.2016.33>
- Vanwonterghem I, Evans PN, Parks DH et al. Methylotrophic methanogenesis discovered in the archaeal phylum *Verstraetearchaeota*. *Nat Microbiol* 2016;**1**:16170. <https://doi.org/10.1038/nmicrobiol.2016.170>
- McKay LJ, Dlakic M, Fields MW et al. Co-occurring genomic capacity for anaerobic methane and dissimilatory sulfur metabolisms discovered in the *Korarchaeota*. *Nat Microbiol* 2019;**4**:614–22. <https://doi.org/10.1038/s41564-019-0362-4>
- Wang Y, Wegener G, Hou J et al. Expanding anaerobic alkane metabolism in the domain of Archaea. *Nat Microbiol* 2019;**4**:595–602. <https://doi.org/10.1038/s41564-019-0364-2>
- Evans PN, Parks DH, Chadwick GL et al. Methane metabolism in the archaeal phylum *Bathyarchaeota* revealed by genome-centric metagenomics. *Science* 2015;**350**:434–8. <https://doi.org/10.1126/science.aac7745>
- Berghuis BA, Yu FB, Schulz F et al. Hydrogenotrophic methanogenesis in archaeal phylum *Verstraetearchaeota* reveals the shared ancestry of all methanogens. *Proc Natl Acad Sci U S A* 2019;**116**:5037–44. <https://doi.org/10.1073/pnas.1815631116>
- Liu YF, Chen J, Zaramela LS et al. Genomic and transcriptomic evidence supports methane metabolism in *Archaeoglobi*. *mSystems* 2020;**5**:e00651–19. <https://doi.org/10.1128/mSystems.00651-19>
- Stetter KO, Lauerer G, Thomm M et al. Isolation of extremely thermophilic sulfate reducers: evidence for a novel branch of

- archaeobacteria. *Science* 1987;**236**:822–4. <https://doi.org/10.1126/science.236.4803.822>
30. Slobodkina G, Allieux M, Merkel A et al. Physiological and genomic characterization of a hyperthermophilic archaeon *Archaeoglobus neptunius* sp. nov. isolated from a deep-sea hydrothermal vent warrants the reclassification of the genus *Archaeoglobus*. *Front Microbiol* 2021;**12**:679245. <https://doi.org/10.3389/fmicb.2021.679245>
  31. Boyd JA, Jungbluth SP, Leu AO et al. Divergent methyl-coenzyme M reductase genes in a deep-subseafloor *Archaeoglobi*. *ISME J* 2019;**13**:1269–79. <https://doi.org/10.1038/s41396-018-0343-2>
  32. Hua ZS, Wang YL, Evans PN et al. Insights into the ecological roles and evolution of methyl-coenzyme M reductase-containing hot spring Archaea. *Nat Commun* 2019;**10**:4574. <https://doi.org/10.1038/s41467-019-12574-y>
  33. Lynes MM, Krukenberg V, Jay ZJ et al. Diversity and function of methyl-coenzyme M reductase-encoding archaea in Yellowstone hot springs revealed by metagenomics and mesocosm experiments. *ISME Commun* 2023;**3**:22. <https://doi.org/10.1038/s43705-023-00225-9>
  34. Wang J, Qu Y-N, Evans PN et al. Evidence for nontraditional *mcr*-containing archaea contributing to biological methanogenesis in geothermal springs. *Sci Adv* 2023;**9**:eadg6004. <https://doi.org/10.1126/sciadv.adg6004>
  35. Buessecker S, Chadwick GL, Quan ME et al. *Mcr*-dependent methanogenesis in *Archaeoglobaceae* enriched from a terrestrial hot spring. *ISME J* 2023;**17**:1649–59. <https://doi.org/10.1038/s41396-023-01472-3>
  36. Laso-Perez R, Krukenberg V, Musat F et al. Establishing anaerobic hydrocarbon-degrading enrichment cultures of microorganisms under strictly anoxic conditions. *Nat Protoc* 2018;**13**:1310–30. <https://doi.org/10.1038/nprot.2018.030>
  37. Brandis A, Thauer RK. Growth of *Desulfovibrio* species on hydrogen and sulphate as sole energy source. *Microbiology* 1981;**126**:249–52. <https://doi.org/10.1099/00221287-126-1-249>
  38. Ai G, Zhu J, Dong X et al. Simultaneous characterization of methane and carbon dioxide produced by cultured methanogens using gas chromatography/isotope ratio mass spectrometry and gas chromatography/mass spectrometry. *Rapid Commun Mass Spectrom* 2013;**27**:1935–44. <https://doi.org/10.1002/rcm.6651>
  39. Bushnell B. *BBMap: A Fast, Accurate, Splice-Aware Aligner*. Berkeley, CA: Lawrence Berkeley National Lab (LBNL), 2014
  40. Seemann T. Prokka: rapid prokaryotic genome annotation. *Bioinformatics* 2014;**30**:2068–9. <https://doi.org/10.1093/bioinformatics/btu153>
  41. Wu Y-W, Tang Y-H, Tringe SG et al. MaxBin: an automated binning method to recover individual genomes from metagenomes using an expectation-maximization algorithm. *Microbiome* 2014;**2**:26. <https://doi.org/10.1186/2049-2618-2-26>
  42. Kang DD, Froula J, Egan R et al. MetaBAT, an efficient tool for accurately reconstructing single genomes from complex microbial communities. *PeerJ* 2015;**3**:e1165. <https://doi.org/10.7717/peerj.1165>
  43. Alneberg J, Bjarnason BS, de Bruijn I et al. Binning metagenomic contigs by coverage and composition. *Nat Methods* 2014;**11**:1144–6. <https://doi.org/10.1038/nmeth.3103>
  44. Miller IJ, Rees ER, Ross J et al. Autometa: automated extraction of microbial genomes from individual shotgun metagenomes. *Nucleic Acids Res* 2019;**47**:e57. <https://doi.org/10.1093/nar/gkz148>
  45. Sieber CMK, Probst AJ, Sharrar A et al. Recovery of genomes from metagenomes via a dereplication, aggregation and scoring strategy. *Nat Microbiol* 2018;**3**:836–43. <https://doi.org/10.1038/s41564-018-0171-1>
  46. Kohtz AJ, Jay ZJ, Lynes MM et al. *Culexarchaeia*, a novel archaeal class of anaerobic generalists inhabiting geothermal environments. *ISME Commun* 2022;**2**:86. <https://doi.org/10.1038/s43705-022-00175-8>
  47. Parks DH, Imelfort M, Skennerton CT et al. CheckM: assessing the quality of microbial genomes recovered from isolates, single cells, and metagenomes. *Genome Res* 2015;**25**:1043–55. <https://doi.org/10.1101/gr.186072.114>
  48. Andrews S, Krueger F, Seconda-Pichon A et al. FastQC: A Quality Control Tool for High Throughput Sequence Data. Babraham Bioinformatics. Babraham Institute, 2015. <https://www.bioinformatics.babraham.ac.uk/projects/fastqc/>
  49. Deng Z-L, Münch PC, Mreches R et al. Rapid and accurate identification of ribosomal RNA sequences via deep learning. *Nucleic Acids Res* 2022;**50**:e60. <https://doi.org/10.1093/nar/gkac112>
  50. Stahl DA. Development and application of nucleic acid probes in bacterial systematics. In: Stackebrandt E., Goodfellow M. (eds.), *Nucleic Acid Techniques in Bacterial Systematics*. Chichester, UK: John Wiley & Sons Ltd, 1991, 205–49
  51. Stetter KO. *Archaeoglobus fulgidus* gen. nov., sp. nov.: a new taxon of extremely thermophilic archaeobacteria. *Syst Appl Microbiol* 1988;**10**:172–3. [https://doi.org/10.1016/S0723-2020\(88\)80032-8](https://doi.org/10.1016/S0723-2020(88)80032-8)
  52. Huber H, Jannasch H, Rachel R et al. *Archaeoglobus veneficus* sp. nov., a novel facultative chemolithoautotrophic hyperthermophilic sulfite reducer, isolated from abyssal black smokers. *Syst Appl Microbiol* 1997;**20**:374–80. [https://doi.org/10.1016/S0723-2020\(97\)80005-7](https://doi.org/10.1016/S0723-2020(97)80005-7)
  53. Mori K, Maruyama A, Urabe T et al. *Archaeoglobus infectus* sp. nov., a novel thermophilic, chemolithoheterotrophic archaeon isolated from a deep-sea rock collected at Suiyo Seamount, Izu-Bonin Arc, western Pacific Ocean. *Int J Syst Evol Micr* 2008;**58**:810–6. <https://doi.org/10.1099/ijs.0.65422-0>
  54. Watkins AJ, Roussel EG, Webster G et al. Choline and N,N-dimethylethanolamine as direct substrates for methanogens. *Appl Environ Microbiol* 2012;**78**:8298–303. <https://doi.org/10.1128/AEM.01941-12>
  55. Hocking WP, Stokke R, Roalkvam I et al. Identification of key components in the energy metabolism of the hyperthermophilic sulfate-reducing archaeon *Archaeoglobus fulgidus* by transcriptome analyses. *Front Microbiol* 2014;**5**:1–20. <https://doi.org/10.3389/fmicb.2014.00095>
  56. Li G, Rabe KS, Nielsen J et al. Machine learning applied to predicting microorganism growth temperatures and enzyme catalytic optima. *ACS Synth Biol* 2019;**8**:1411–20. <https://doi.org/10.1021/acssynbio.9b00099>
  57. Mahapatra A, Patel A, Soares JA et al. Characterization of a *Methanosarcina acetivorans* mutant unable to translate UAG as pyrrolysine. *Mol Microbiol* 2006;**59**:56–66. <https://doi.org/10.1111/j.1365-2958.2005.04927.x>
  58. Ferguson T, Soares JA, Lienard T et al. Rama, a protein required for reductive activation of corrinoid-dependent methylamine methyltransferase reactions in methanogenic archaea. *J Biol Chem* 2009;**284**:2285–95. <https://doi.org/10.1074/jbc.M807392200>
  59. Estelmann S, Ramos-Vera WH, Gad'on N et al. Carbon dioxide fixation in '*Archaeoglobus lithotrophicus*': are there

- multiple autotrophic pathways? *FEMS Microbiol Lett* 2011;**319**: 65–72. <https://doi.org/10.1111/j.1574-6968.2011.02268.x>
60. Ferry JG. How to make a living by exhaling methane. *Annu Rev Microbiol* 2010;**64**:453–73. <https://doi.org/10.1146/annurev.micro.112408.134051>
61. Chernykh NA, Neukirchen S, Frolov EN et al. Dissimilatory sulfate reduction in the archaeon '*Candidatus Vulcanisaeta moutnovskia*' sheds light on the evolution of sulfur metabolism. *Nat Microbiol* 2020;**5**:1428–38. <https://doi.org/10.1038/s41564-020-0776-z>
62. Neukirchen S, Sousa FL. DiSCo: a sequence-based type-specific predictor of Dsr-dependent dissimilatory sulphur metabolism in microbial data. *Microb Genom* 2021;**7**:000603. <https://doi.org/10.1099/mgen.0.000603>
63. Ramos AR, Keller KL, Wall JD et al. The membrane QmoABC complex interacts directly with the dissimilatory adenosine 5'-phosphosulfate reductase in sulfate reducing bacteria. *Front Microbiol* 2012;**3**:137. <https://doi.org/10.3389/fmicb.2012.00137>
64. Adams MWW. The metabolism of hydrogen by extremely thermophilic, sulfur-dependent bacteria. *FEMS Microbiol Rev* 1990;**75**:219–37. <https://doi.org/10.1111/j.1574-6968.1990.tb04096.x>
65. Ma K, Schicho RN, Kelly RM et al. Hydrogenase of the hyperthermophile *Pyrococcus furiosus* is an elemental sulfur reductase or sulphydrogenase: evidence for a sulfur-reducing hydrogenase ancestor. *Proc Natl Acad Sci U S A* 1993;**90**:5341–4. <https://doi.org/10.1073/pnas.90.11.5341>
66. Hocking WP, Roalkvam I, Magnussen C et al. Assessment of the carbon monoxide metabolism of the hyperthermophilic sulfate-reducing archaeon *Archaeoglobus fulgidus* VC-16 by comparative transcriptome analyses. *Archaea* 2015;**2015**:235384. <https://doi.org/10.1155/2015/235384>
67. Welte C, Deppenmeier U. Membrane-bound electron transport in *Methanosaeta thermophila*. *J Bacteriol* 2011;**193**:2868–70. <https://doi.org/10.1128/JB.00162-11>
68. Pereira IA, Haveman SA, Voordouw G. Biochemical, genetic and genomic characterization of anaerobic electron transport pathways in sulphate-reducing Delta-proteobacteria. In: Barton L.L., Hamilton W.A. (eds.), *Sulphate-Reducing Bacteria: Environmental and Engineered Systems*. Cambridge, UK: Cambridge University Press, 2007, 215–40
69. Grein F, Pereira IA, Dahl C. Biochemical characterization of individual components of the *Allochromatium vinosum* DsrMKJOP transmembrane complex aids understanding of complex function in vivo. *J Bacteriol* 2010;**192**:6369–77. <https://doi.org/10.1128/JB.00849-10>
70. Wu K, Zhou L, Tahon G et al. Isolation of a methyl-reducing methanogen outside the Euryarchaeota. 2023. <https://doi.org/10.21203/rs.3.rs-2501667/v1>
71. Kohtz A, Krukenberg V, Petrosian N et al. Cultivation and visualization of a methanogen of the phylum *Thermoproteota*. 2023. <https://doi.org/10.21203/rs.3.rs-2500102/v1>
72. Spang A, Caceres EF, Ettema TJG. Genomic exploration of the diversity, ecology, and evolution of the archaeal domain of life. *Science* 2017;**357**:eaaf3883. <https://doi.org/10.1126/science.aaf3883>

## Supporting Information

### **SI Results and Discussion**

#### **Protologue**

*Methanoglobus hypatiae* sp. nov.

Me.tha.no.glo.bus. Gr. pref. *methano-*, pertaining to methane; L. masc. n. *-globus*, sphere; Gr.L. masc. n. *Methanoglobus*, methane producing organism spherical in shape. This genus was named by Buessecker *et al.* (17). Hy.pa.ti.ae. Gr. fem. *hypatiae*, to honor Hypatia of Alexandria, a respected and renowned philosopher of ancient Alexandria, Egypt, who made significant contributions to the understanding of mathematics and astronomy. A symbol of intellectual courage and scholarly achievement. This archaeon was cultured from an unnamed hot spring in the Lower Culex Basin of Yellowstone National Park identified as feature LCB024 (1). This archaeon is an obligately anaerobic thermophile that performs methylotrophic methanogenesis using methylamines and grows as regular to irregular coccoid cells approximately 0.5 to 1  $\mu\text{m}$  in width. The type genome of this archaeon is deposited at NCBI under BioProject PRJNA1014417, accession number will be added upon publication.

### **SI Materials and Methods**

#### **Amplicon Sequencing and Analysis**

DNA was extracted from environmental slurry samples and enrichment cultures sampled on the day of transfer using the FastDNA Spin Kit for Soil (MP Biomedicals, Irvine, CA) following the manufacturer's guidelines. Archaeal and bacterial 16S rRNA genes were amplified with the updated Earth Microbiome Project primer set 515F and 806R (18). Amplicon libraries were prepared as previously described (1) and sequenced by the Molecular Research Core Facility at Idaho State University (Pocatello, ID) using an Illumina MiSeq platform with 2 x 250 bp paired end read chemistry. Gene reads were processed using QIIME 2 version 2022.8 (19). Primer sequences were removed from demultiplexed reads using cutadapt (20) with error rate 0.12 and reads truncated (130 bp forward, 150 bp reverse), filtered, denoised and merged in DADA2 with default settings (21). Processed 16S rRNA gene amplicon sequence variants (ASVs) were taxonomically classified with the sklearn method and the SILVA 138 database (22). The R package *decontam* (version 1.18.0) (23) was used to remove contaminants using the "Prevalence" model with a threshold of 0.5.

#### **Annotation and Reconstruction of Metabolic Potential**

Genes associated with methanogenesis pathways, dissimilatory sulfur metabolism pathways, coenzyme and cofactor biosynthesis, energy conservation, and beta-oxidation, were inventoried. Annotations assigned by Prokka were refined through manual evaluation using KofamKOALA, NCBI BLASTP, NCBI's Conserved Domain Database, InterPro, the hydrogenase classifier HydDB, and DiSCo (24-29).

#### **Phylogenetic and Phylogenomic Analyses**

Average nucleotide identities (ANI) of 16S rRNA genes were calculated with blastn, with ANI and average amino acid identities (AAI) calculated by pyani v02.2.12 (ANIb) and CompareM v0.0.23 (--fragLen 2000) (<https://github.com/dparks1134/CompareM>), respectively for selected Archaeoglobales genomes and MAGs (Table 1). Phylogenetic analysis of 16S rRNA genes was performed with fasttree (30) using masked alignments generated by ssu-align.

Archaeoglobales MAGs and reference genomes were screened for 54 phylogenetically informative single copy proteins (31, 32) of which a subset of 33 proteins were identified in them all (SI Appendix, Table S4). In order to maximize the number of proteins compared across references, MAGs LMO1 and LMO3 were excluded from this analysis, as they lacked 2 and 7 proteins out of the total 33, respectively. These were then aligned with muscle (33), concatenated, and phylogenomically analyzed with maximum likelihood analysis with fasttree (WAG model). McrA alignments were performed with MAFFT-LINSi v7.522 (34), trimmed with trimAL v1.4.rev22 (35) using a 0.5 gap threshold, and maximum likelihood trees were built with IQTree2 v2.0.6 (36) using LG+C60+F+G model and 1,000 ultrafast bootstraps.

### **Temperature and Substrate Optimum Experiments**

Methane production and growth of *Archaeoglobus* was evaluated at different temperatures and in the presence of methylated substrates (i.e., methanol and mono-, di-, and trimethylamine), lactate, and media prepared without yeast extract. The sixth transfer of the enrichment was used to inoculate triplicate 30 mL serum bottles containing 15 mL of medium with 8% v/v inoculum, streptomycin (50 mg/L), vancomycin (50 mg/L), and 10 mM of each substrate tested. Cultures were evaluated at 60°C, 64°C, 70°C, 77°C, 80°C, and 85°C with 10 mM MMA. Separately, we tested whether the culture would grow on the following substrate (combinations): 10 mM dimethylamine (DMA); 10 mM trimethylamine (TMA); 10 mM methanol (MeOH); 10 mM lactate (LAC); 10 mM MMA and 10 mM LAC); 10 mM MMA with media without yeast extract; and a control in media without yeast or any methanogenic substrate. The 70°C cultures amended with 10 mM MMA served as the control. All incubations were performed in biological triplicate.

### **Methane Measurements**

During cultivation, 250 µL subsamples of the headspace were taken using a gas tight syringe (Hamilton) and injected into a 10 mL autosampler vial that had been sealed with grey chlorobutyl septa. Samples were taken from the autosampler vials and injected into a Shimadzu 2020-GC gas chromatograph equipped with a GS-CarbonPLOT column (30 m x 0.32 mm; 1.5 µm film thickness; Agilent) and a Rt-Q-BOND column (30 m x 0.32 mm; 1.5 µm film thickness; Restek) using helium as a carrier gas. All injections were performed by a Shimadzu AOC-6000 autosampler robot. The injector, column, and flame ionization detector (FID) were maintained at 200°C, 50°C, and 240°C, respectively. Methane concentrations were calculated based on injection of a standard curve.

### **Fluorescence *in situ* hybridization and cell counts**

Aliquots of enrichment cultures incubated with <sup>13</sup>C-MMA during the SIT experiment were treated with 2% paraformaldehyde (PFA) and fixed for 1 hr at room temperature. Following fixation, cells were washed twice with 1x PBS, followed by centrifugation at 16,000 × g to remove the supernatant, resuspended in 1x PBS, and stored at 4°C. For direct cell counts, aliquots of fixed cell suspensions were filtered onto polycarbonate filters (0.2 µm pore size, 25 mm diameter, GTTP Millipore, Germany) and air dried before filter pieces were cut and embedded in 0.2% low melting agarose. We attempted to use the Archaeoglobales-specific probe Arglo32 (37), however fluorescent signal was insufficient. Given *Ca. M. hypatiae* was the sole archaeon in the enrichment culture, the relative abundance of *Ca. M. hypatiae* cells was determined via catalyzed reporter deposition fluorescence *in situ* hybridization (CARD-FISH) using the general archaea-targeted 16S rRNA oligonucleotide probe Arch915 (38). Total cell counts were based on DNA-stained cells using DAPI (4,6-diamidino-2-phenylindole). CARD-FISH was performed as previously described (39). Cell wall permeabilization was achieved with a brief treatment of 0.1 M HCl (1

min, RT) followed by treatment with 0.01 M HCl (15 min, RT). Endogenous peroxidases were inactivated with 0.15% H<sub>2</sub>O<sub>2</sub> in methanol (30 min, RT). A formamide concentration of 35% was used for all hybridization reactions (2.5 hrs, 46°C). CARD was performed using Alexa Fluor 594 labeled tyramides for 30 min at 46°C. Following signal amplification, an additional washing step in 1x PBS was included to reduce background fluorescence (15 min, RT, dark). Samples were stained with DAPI, embedded in Citifluor-Vectashield, and enumerated using an epifluorescence microscope (Leica DM4B).

### **Scanning electron microscopy (SEM)**

An aliquot of the enrichment culture at transfer 7 (T7) was treated with 2% paraformaldehyde (PFA) and fixed for 1 hr at room temperature. Following fixation, cells were washed twice through centrifugation at 16,000 × g to remove the supernatant, resuspended in 1x phosphate buffered saline (PBS), and stored at 4°C. Samples for imaging were prepared according to Schaible et al., 2022 (40). Briefly, a square coupon of mirror-finished 304 stainless steel (25 mm diameter, 0.6 mm thickness) was purchased from Stainless Supply (Monroe, NC). The coupon was cleaned by washing with a 1% solution of Tergazyme (Alconox, New York, NY) and rinsed with Milli-Q water. The coupon was dried under compressed air and stored at room temperature. 5 µL of fixed sample was spotted on the coupon and air-dried at 46 °C for 3 min. The coupon was then dried for 1 m each step in a successive ethanol series starting with 10% ethanol and increasing by increments of 10% with the last step 90% ethanol. SEM images were captured using a Zeiss (Jena, Germany) SUPRA 55VP field emission scanning electron microscope (FE-SEM). The microscope was operated at 1 keV under a vacuum of 0.2–0.3 mPa, with a working distance of 5.4–6.2 mm at the Imaging and Chemical Analysis Laboratory (ICAL) of Montana State University (Bozeman, MT). No conductivity coating was applied before SEM analysis as the microscope was operated at 1 keV.

## **SI Tables**

**Table S1.** Extended community composition history of methanogenic enrichment cultures via estimated relative abundance (%) from 16S rRNA gene amplicon sequencing.

	<b>LCB024 sediment</b>	<b>Slurry 11/2021</b>	<b>Slurry 02/2022</b>	<b>Initial Enrichment</b>	<b>T1</b>	<b>T2</b>	<b>T3</b>	<b>T4</b>	<b>T4 - MG</b>	<b>T5</b>	<b>SIT- MG</b>
Archaeoglobaceae ASV_78ad2	0.46	0.32	0.02	6.42	74.8	68.9	48.5	46.0	84.7	62.2	92.8
Pseudothermotoga ASV_17231	2.14	1.06	1.08	18.93	6.8	17.1	28.5	37.4	14.5	15.7	3.2
Other Archaeoglobaceae uncultured	0.00	0.00	0.00	1.54	0.0	0.01	0.0	0.0	0.0	0.0	0.0
Confirmed methanogenic archaea	0.25	0.38	0.45	0.00	0.0	0.0	0.0	0.0	0.0	0.0	0.0
Other Archaea	13.51	11.87	10.49	2.67	0.0	0.0	0.0	0.04	0.0	0.0	0.0
Other Bacteria	83.63	86.37	87.95	70.44	18.4	14.1	23.1	16.5	0.8	22.1	4.0



**Table S2.** Methane production of the enrichment culture over time. T, transfer.

Culture ID	Days continuous	Days	CH <sub>4</sub> (μM)	CH <sub>4</sub> (mM)	CH <sub>4</sub> (ppm)	CH <sub>4</sub> (%)
<b>1A – initial enrichment</b>	6	6	4.91	0.00	118.67	0.01
	13	13	16.73	0.02	404.73	0.04
	20	20	12.98	0.01	314.13	0.03
	27	27	12.86	0.01	311.20	0.03
	36	36	32.92	0.03	796.48	0.08
	48	48	146.28	0.15	3538.80	0.35
	53	53	279.15	0.28	6753.17	0.68
	63	63	419.11	0.42	10139.33	1.01
	70	70	447.12	0.45	10816.36	1.08
<b>T1</b>	82	12	14.40	0.01	348.40	0.03
	91	21	50.85	0.05	1230.06	0.12
	98	27	198.41	0.20	4800.09	0.48
	106	35	390.47	0.39	9445.97	0.94
	113	42	565.32	0.57	13676.04	1.37
	117	46	688.44	0.69	16654.06	1.67
	126	55	1442.03	1.44	34885.74	3.49
	133	62	1844.13	1.84	44611.75	4.46
<b>T2</b>	146	7	15.22	0.02	368.32	0.04
	158	18	16.11	0.02	389.83	0.04
	175	34	49.40	0.05	1195.06	0.12
	197	57	680.54	0.68	16463.41	1.65
	221	81	2200.24	2.20	53227.90	5.32
	229	89	2654.34	2.65	64213.66	6.42
	238	98	2230.72	2.23	53964.66	5.40
<b>T3</b>	243	5	18.17	0.02	439.53	0.04
	259	21	10.70	0.01	258.82	0.03
	266	28	536.13	0.54	12969.71	1.30
	274	36	2413.23	2.41	58379.47	5.84
	280	42	2283.95	2.28	55253.34	5.53
	284	46	2193.96	2.19	53077.04	5.31
<b>T4</b>	294	10	17.36	0.02	420.07	0.04
	301	17	18.12	0.02	438.37	0.04
	309	25	12.51	0.01	302.54	0.03
	319	35	1944.01	1.94	47028.08	4.70
	327	43	3054.00	3.05	73881.94	7.39
	335	51	2619.45	2.62	63370.12	6.34
<b>T5</b>	347	10	13.41	0.01	324.42	0.03
	355	18	13.14	0.01	317.78	0.03
	365	28	137.59	0.14	3328.60	0.33
	371	34	1023.35	1.02	24756.27	2.48
	375	38	2218.75	2.22	53674.81	5.37
	384	46	2459.29	2.46	59493.85	5.95
<b>T6</b>	386	2	16.29	0.02	394.19	0.04
	393	9	21.33	0.02	516.14	0.05
	400	16	18.68	0.02	451.92	0.05
	407	23	245.86	0.25	5947.76	0.59
	412	28	2555.27	2.56	61815.61	6.18
	414	30	3432.93	3.43	83051.24	8.31
	416	32	3621.90	3.62	87623.79	8.76
	418	34	3942.97	3.94	95385.88	9.54
<b>T7</b>	428	9	34.33	0.03	830.38	0.08
	435	16	296.91	0.30	7182.55	0.72
	440	21	2931.05	2.93	70907.06	7.09
	444	25	3164.45	3.16	76553.52	7.66
	446	27	3338.04	3.34	80751.55	8.08

**Table S3.** Extended Archaeoglobales metagenome assembled genome and isolate genome statistics (1-16). A combined assembly of metagenomes from T4-MG and SIT-MG (Fig. 1A) for the *Ca. M. hypatiatae* LCB24 MAG was used as it yielded an improved assembly. GTDB classified the YNP, GBS, and China MAGs as: d\_Archaea;p\_Halobacteriota;c\_Archaeoglobales;f\_Archaeoglobales;g\_WYZ-LMO2;s\_WYZ-LMO2. Len., length; Compl., completeness; Redun, redundancy; Strain Hetero., strain heterogeneity; pOGT, predicted optimal growth temperature. \* stop codon interrupts *mcrA* sequence; <sup>a</sup> Both sequences 5' start; not identical; <sup>b</sup> Consists of 1 chromosome and 1 plasmid.

	Seqs	Len (Mb)	GC (%)	Compl. (%)	Redun. (%)	16S	tRNA	CDS	<i>mcrA</i>	CRISPRs	pOGT (°C)	Citation
<b><i>Ca. M. hypatiatae</i> LCB24</b>	19	1.624	46.12	100	1.31	1	44	1,760	1	2	74.44	This study
Archaeoglobales LCB024-003	179	1.157	45.72	88.48	1.31	0	31	1,226	1	1	73.90	Lynes <i>et al.</i> 2023
Archaeoglobales WYZ-LMO2	220	1.514	45.92	97.60	0	0	40	1,614	1	2	72.40	Wang <i>et al.</i> 2019
<i>Ca. M. hydrogenotrophicum</i> bin/74	127	1.547	45.63	92.81	1.31	1	34	1,679	0*	9	75.32	Liu <i>et al.</i> 2020
Archaeoglobales SJ3.Bin34	73	1.468	46.00	98.69	0.65	0	39	1,581	1	2	73.13	Colman <i>et al.</i> 2019
<i>Ca. Methanoglobus nevadensis</i> GBS	71	1.602	47.16	98.04	3.66	1	47	1,785	1	2	74.75	Peacock <i>et al.</i> 2013
Archaeoglobales GMQP bin32	20	1.727	41.26	100	0.98	1	39	1,931	1	2	71.88	Hua <i>et al.</i> 2019
Archaeoglobales GMQP_D bin 18	22	1.565	42.01	97.39	0.98	1	45	1,747	1	3	69.41	Wang <i>et al.</i> 2023
Archaeoglobales JZ-3 D bin 138	32	1.550	42.08	99.35	1.31	1	43	1,701	1	2	69.11	Wang <i>et al.</i> 2023
Archaeoglobales WYZ-LMO1	140	1.557	43.85	88.89	1.31	1	41	1,701	1	1	72.72	Wang <i>et al.</i> 2019
Archaeoglobales WYZ-LMO3	135	1.568	43.93	88.03	1.96	2 <sup>a</sup>	35	1,670	1	2	73.09	Wang <i>et al.</i> 2019
<i>Ca. M. hydrogenotrophicum</i> bin11	252	1.220	47.59	91.83	6.17	1	27	1,387	1	0	72.64	Liu <i>et al.</i> 2020
<i>Ca. M. hydrogenotrophicum</i> bin16	46	1.668	45.49	96.51	1.31	0	41	1,864	1	2	72.69	Liu <i>et al.</i> 2020
Archaeoglobus JZ bin24	35	1.492	44.66	99.35	1.31	0	44	1,642	0	2	68.52	unpublished
Archaeoglobales LCB024-002	66	1.334	42.28	97.39	0.03	0	41	1,459	0	0	73.46	Lynes <i>et al.</i> 2023
Archaeoglobales LCB003-04	128	1.335	42.27	96.73	1.96	0	38	1,447	0	0	73.71	Lynes <i>et al.</i> 2023
Archaeoglobales SJ3 bin61	45	1.270	41.68	89.54	0	1	40	1,392	0	0	73.34	Colman <i>et al.</i> 2019
Archaeoglobales JZ_75 SW bin109	16	1.562	39.48	99.35	0.65	1	45	1,762	1	5	74.34	Wang <i>et al.</i> 2023
<i>Archaeoglobus fulgidus</i> DSM 4304	1	2.178	48.58	100	0	1	46	2,440	0	3	79.88	Klenk <i>et al.</i> 1997
<i>Archaeoglobus neptunius</i> SE56	32	2.116	46.05	100	0	1	47	2,336	0	2	78.26	Slobodkina <i>et al.</i> 2021
<i>Archaeoglobus profundus</i> DSM 5631	2 <sup>b</sup>	1.563	46.05	100	0	1	48	1,784	0	0	85.86	von Jan <i>et al.</i> 2010
<i>Ferrolobus placidus</i> DSM 10642	1	2.196	44.14	100	0	1	49	2,467	0	1	83.83	Anderson <i>et al.</i> 2011
<i>Geoglobus acetivorans</i> SBH6	1	1.861	46.84	99.84	0	1	48	2,168	0	6	78.22	Mardanov <i>et al.</i> 2015
<i>Geoglobus ahangari</i> 234	1	1.770	53.11	100	0	1	46	1,985	0	7	84.11	Manzella <i>et al.</i> 2015
<i>Archaeoglobus sulfatocaldus</i> PM70-1	1	2.077	43.24	100	0	1	51	2,237	0	1	76.12	Stokke <i>et al.</i> 2013
<i>Archaeoglobus veneficus</i> SNP6	1	1.902	47.05	99.35	0	1	46	2,055	0	2	76.18	Mukherjee <i>et al.</i> 2017
<i>Ca. Polytropus marinfundus</i> rG16	21	2.129	40.22	99.84	1.96	1	44	2,286	2	0	66.39	Boyd <i>et al.</i> 2019

**Table S4.** Conserved single copy proteins used in phylogenomic analysis of MAGs and isolates.

<b>arCOG</b>	<b>Gene</b>	<b>Product</b>
arCOG00405	GRS1	Glycyl-tRNA synthetase (class II)
arCOG00779	RplO	Ribosomal protein L15
arCOG00785	RpmC	Ribosomal protein L29
arCOG01001	Map	Methionine aminopeptidase
arCOG01183	Kae1p/TsaD	Subunit of KEOPS complex, contains a domain with ASKHA fold and RIO-type kinase (AP-endonuclease activity)
arCOG01228	Ffh	Signal recognition particle GTPase
arCOG01722	RpsM/rps13p	Ribosomal protein S13
arCOG01758	RpsJ/rps10p	Ribosomal protein S10
arCOG04070	RplC	Ribosomal protein L3
arCOG04071	RplD	Ribosomal protein L4
arCOG04072	RplW	Ribosomal protein L23
arCOG04086	RpmD	Ribosomal protein L30
arCOG04087	RpsE	Ribosomal protein S5
arCOG04088	RplR	Ribosomal protein L18
arCOG04090	RplF/rpl6p	Ribosomal protein L6P
arCOG04091	RpsH/rps8p	Ribosomal protein S8
arCOG04094	RplX/rpl24p	Ribosomal protein L24
arCOG04095	RplN/rps14p	Ribosomal protein L14
arCOG04096	RpsQ/rps17p	Ribosomal protein S17
arCOG04097	RpsC/rps3p	Ribosomal protein S3
arCOG04098	RplV/rpl22p	Ribosomal protein L22
arCOG04113	RplP	Ribosomal protein L10AE/L16
arCOG04121	RnhB	Ribonuclease HII
arCOG04169	SecY	Preprotein translocase subunit SecY
arCOG04185	RpsO	Ribosomal protein S15P
arCOG04239	RpsD/rps4p	Ribosomal protein S4 or related protein
arCOG04242	RplM/rpl13p	Ribosomal protein L13
arCOG04243	RpsI/rps9p	Ribosomal protein S9
arCOG04245	RpsB/rps2p	Ribosomal protein S2
arCOG04255	RpsL/rps12p	Ribosomal protein S12
arCOG04256	RpoC/Rpo11	DNA-directed RNA polymerase subunit A''
arCOG04257	RpoC/Rpo3/rpoA1	DNA-directed RNA polymerase subunit A'
arCOG04277	Efp	Translation elongation factor P (EF-P)/translation initiation factor 5A (eIF-5A)

**Table S5.** Calculated cell density of replicates in the SIT experiment. FID measurements of replicates used to determine cell density. Density is calculated based on cell counts of DAPI and CARD-FISH labeled samples. Stdev., standard deviation. Letters A-F identify each replicate.

Summary	<sup>12</sup> CH <sub>4</sub>		Cell Density, cells mL <sup>-1</sup>		% labeled with Arch915
	μM	ppm	DAPI	FISH	
5A Day 22	25	610	3.83 × 10 <sup>7</sup>	1.34 × 10 <sup>6</sup>	3.5
5B Day 22	57	1,374	1.88 × 10 <sup>7</sup>	5.07 × 10 <sup>6</sup>	12.7
5E Day 22	50	1,204	3.49 × 10 <sup>7</sup>	0	0
5F Day 22	132	3,196	4.59 × 10 <sup>7</sup>	2.21 × 10 <sup>6</sup>	4.8
<b>Day 22 Average</b>	66	1,596	3.45 × 10 <sup>7</sup>	2.16 × 10 <sup>6</sup>	5.3
<b>Day 22 Stdev.</b>	46	1,116	1.14 × 10 <sup>7</sup>	2.15 × 10 <sup>6</sup>	5.4
5A Day 32	741	17,917	4.26 × 10 <sup>7</sup>	2.85 × 10 <sup>7</sup>	66.9
5B Day 32	2,176	52,635	1.11 × 10 <sup>8</sup>	6.00 × 10 <sup>7</sup>	54.2
5E Day 32	1,779	43,035	3.40 × 10 <sup>7</sup>	1.74 × 10 <sup>7</sup>	51.2
5F Day 32	2,412	58,355	9.14 × 10 <sup>7</sup>	4.03 × 10 <sup>7</sup>	44.1
<b>Day 32 Average</b>	1,777	42,985	6.97 × 10 <sup>7</sup>	3.65 × 10 <sup>7</sup>	54.1
<b>Day 32 Stdev.</b>	739	17,868	3.73 × 10 <sup>7</sup>	1.82 × 10 <sup>7</sup>	9.6
5A Day 45	4,109	99,398	12.2 × 10 <sup>7</sup>	6.41 × 10 <sup>7</sup>	52.7

## SI Figures

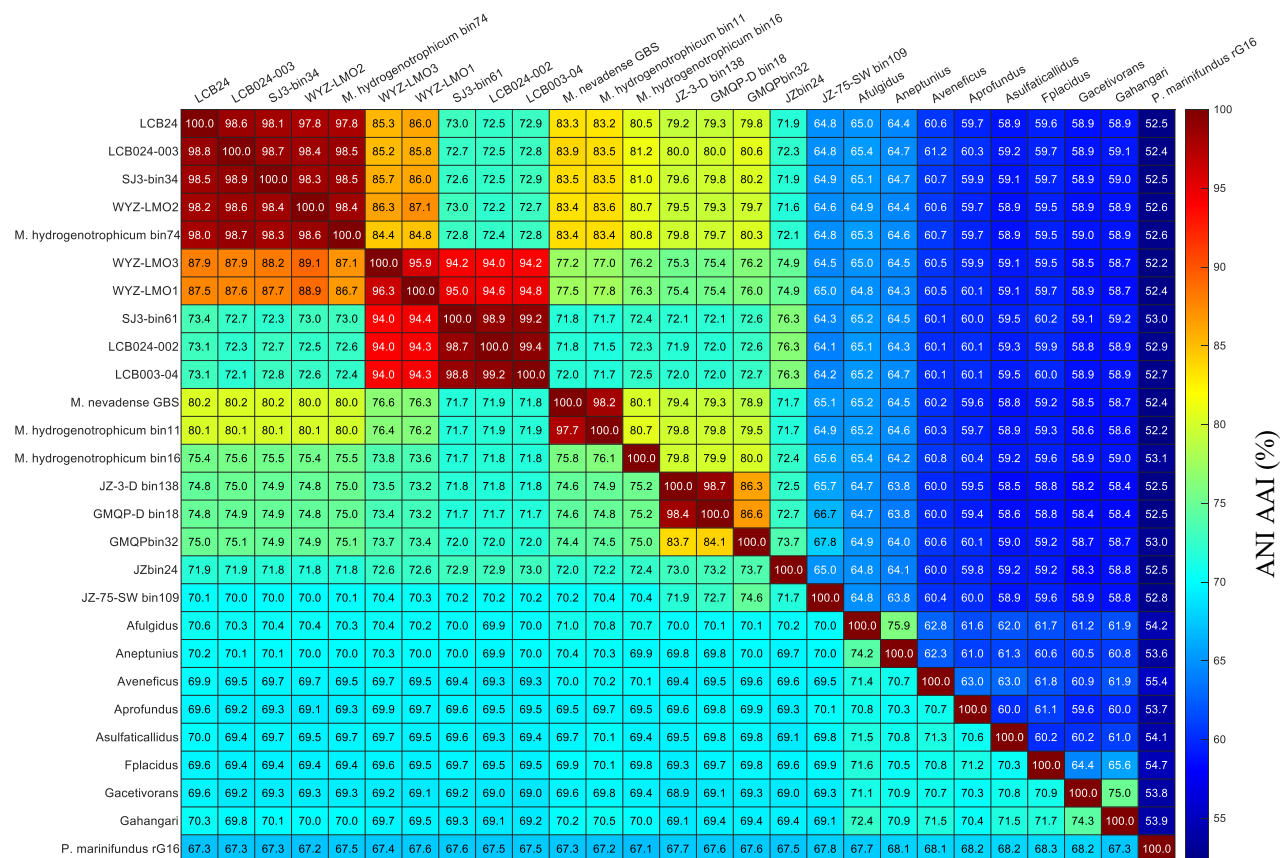


**Fig. S1.** Detailed ANI (lower half of matrix) and AAI (upper half of matrix) analysis of related Archaeoglobales MAGs and reference genomes.

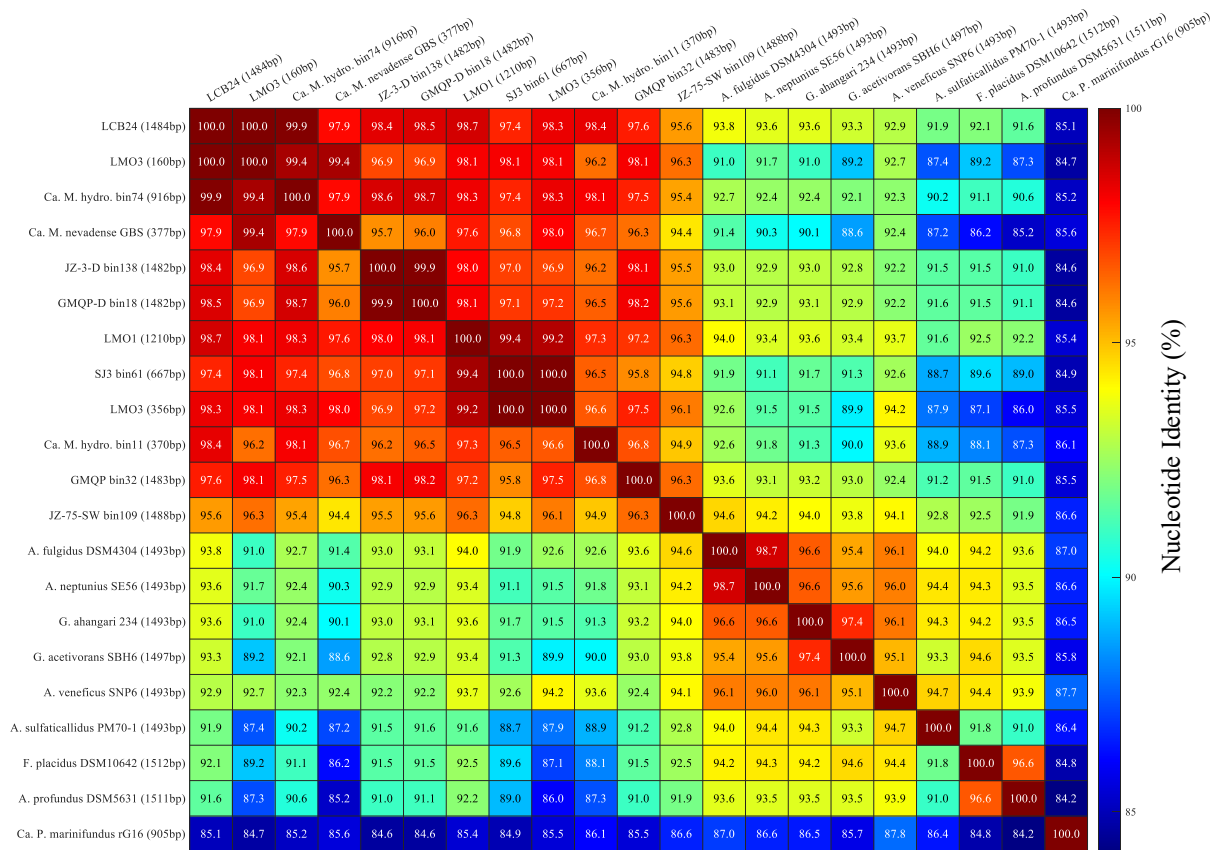


**Fig. S2.** 16S rRNA nucleotide identity analysis of closely related Archaeoglobales MAGs and reference genomes.

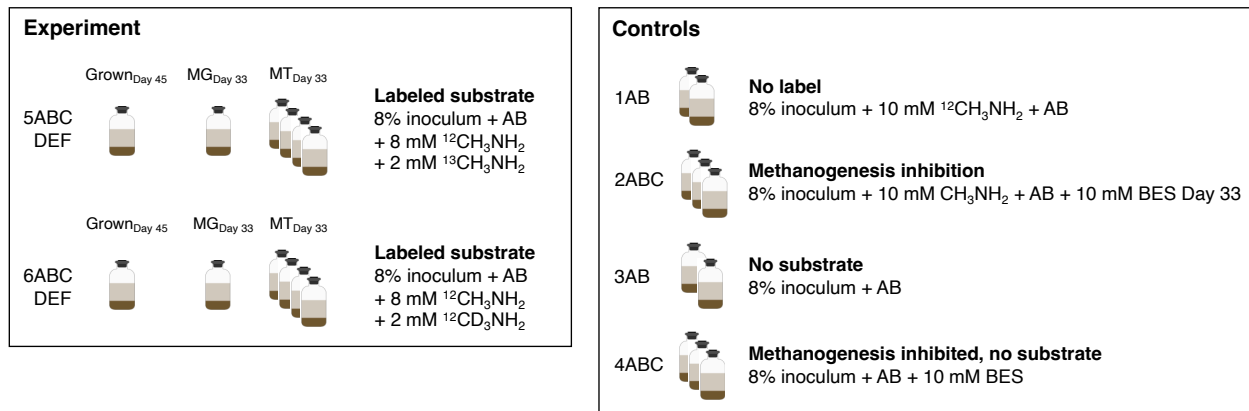


**Fig. S3.** Experimental setup of the stable isotope tracing (SIT) experiment. Incubations were carried out in 30 mL culture volumes in 60 mL serum bottles with 8% v/v inoculum, 50 mg/L streptomycin, 50 mg/L vancomycin, 10 mM MMA, and  $\text{N}_2$  gas (99.999%) incubated in anoxic media (pH 7.8, 70°C). Replicates sacrificed for analysis during mid-log phase are indicated. Of the eight samples harvested for metatranscriptomics, six were sequenced and used for analysis as two replicates did not yield sufficient RNA for sequencing. AB, antibiotics streptomycin and vancomycin, MG, metagenome sample; MT, metatranscriptome sample; BES, bromoethanesulfonate/methanogenesis inhibitor.

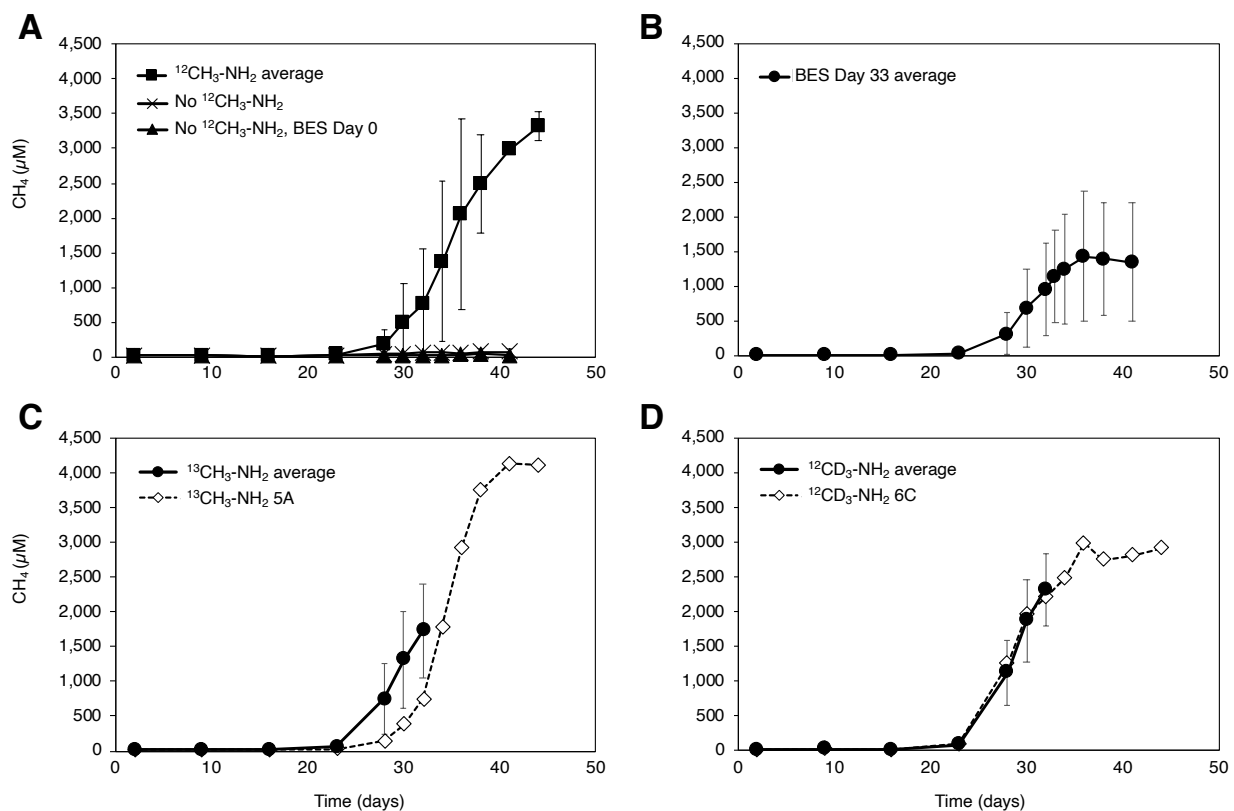


**Fig. S4.**  $^{12}\text{CH}_4$  measurements by GC-FID during the stable isotope tracing experiment. Measurements can be found in Dataset S3.



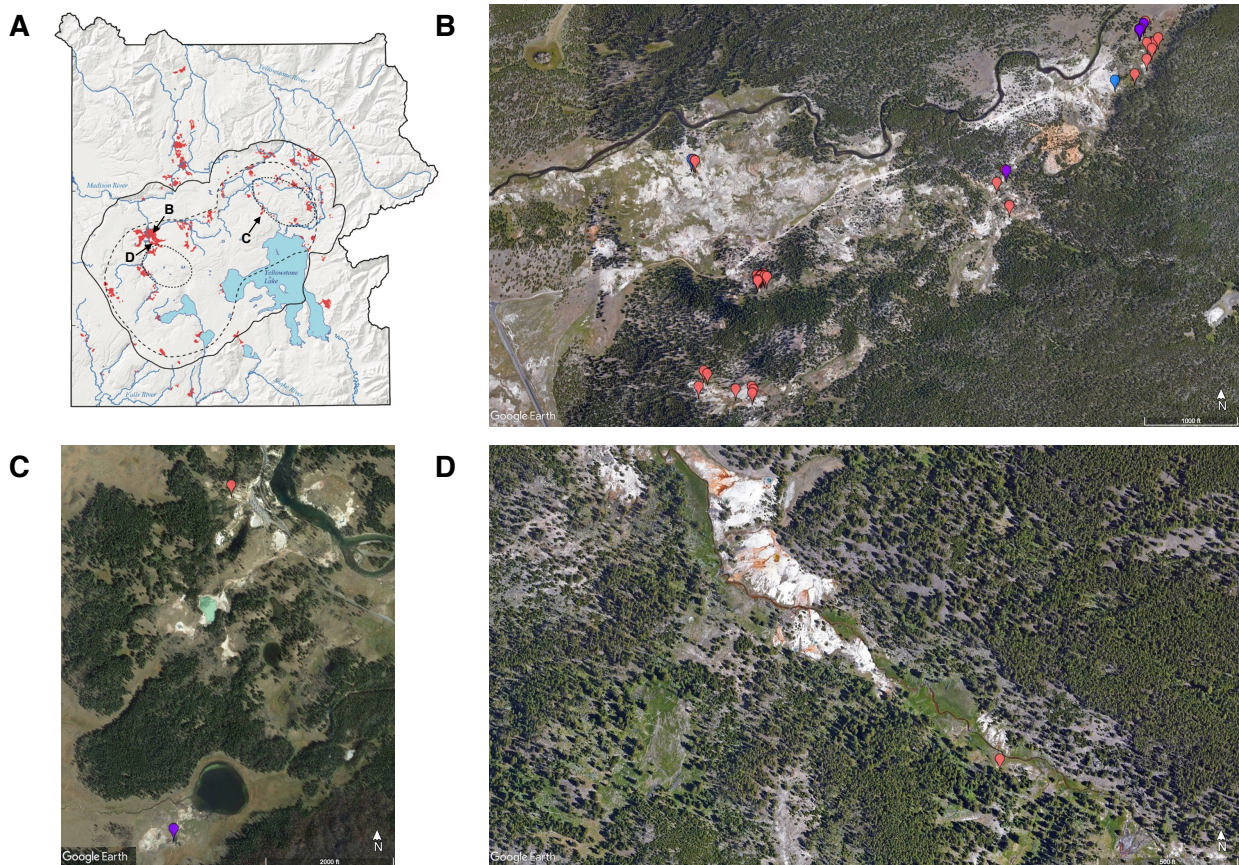


**Fig. S5.** Geographical distribution of geothermal features in Yellowstone National Park in which *Archaeoglobi*-related *mcrA* genes ( $n = 36$ ) and *Ca. M. hypatiae*-related 16S rRNA genes ( $n = 6$ ) were detected. Features are located in the (A) Map of Yellowstone National Park Wyoming, USA modified from Vaughan *et al.* 2014 (41) (B) Lower Culex Basin ( $n = 36$ ), (C) Mud Volcano Region ( $n = 2$ ), and (D) the White Creek Area ( $n = 1$ ). These features spanned a wide pH (2.61-9.35) and temperature (18.4-93.8 °C) range. Features in which *mcrA* were detected are marked in red and features with related 16S rRNA genes are shown in blue. Features in which both amplicons were detected are colored in purple. For details on these sites, their *mcrA* data, water geochemistry, and exact location, see Lynes & Krukenberg *et al.*, 2023. Image source: Google Earth.

## **Description of Available Supplementary Datasets**

**SI Dataset S1.** Extended metagenome assembled genome (SIT-MG) and isolate genome statistics. Seqs, sequences; avg\_cov, average coverage; avg\_gc, average G+C content; % rel. abund., percent relative abundance.

**SI Dataset S2.** GCMS measurements of masses 16 (CH<sub>4</sub>), 17 (<sup>13</sup>CH<sub>4</sub>), and 19 (<sup>12</sup>CD<sub>3</sub>H) during the isotope tracing experiment. Percent of labeled methane is calculated as a fraction of provided labeled substrate. Stdev, standard deviation.

**SI Dataset S3.** Gas chromatograph FID measurements of <sup>12</sup>CH<sub>4</sub> during isotope tracing experiment. NA, not available/measured.

**SI Dataset S4.** Gas chromatograph FID measurements of CH<sub>4</sub> during temperature optimum experiment. NA, not available/measured.

**SI Dataset S5.** Inventory of genes expressed by *Ca. M. hypatiae* LCB24 under methanogenic conditions and as depicted in Fig. 5. Expression levels averaged across six replicates are reported in reads per kilobase of transcript per million mapped reads (RPKM).

**SI Dataset S6.** Inventory of genes expressed by *Ca. M. hypatiae* LCB24 under methanogenic conditions belonging to the beta-oxidation pathway. Expression levels averaged across six replicates are reported in reads per kilobase of transcript per million mapped reads (RPKM).

## References

1. Lynes MM, Krukenberg V, Jay ZJ, Kohtz AJ, Gobrogge CA, Spietz RL, et al. Diversity and function of methyl-coenzyme M reductase-encoding archaea in Yellowstone hot springs revealed by metagenomics and mesocosm experiments. *ISME Commun.* 2023;3:22.
2. Wang Y, Wegener G, Hou J, Wang F, Xiao X. Expanding anaerobic alkane metabolism in the domain of Archaea. *Nat Microbiol.* 2019;4:595-602.
3. Liu YF, Chen J, Zaramela LS, Wang LY, Mbadanga SM, Hou ZW, et al. Genomic and transcriptomic evidence supports methane metabolism in *Archaeoglobi*. *mSystems.* 2020;5:e00651-19.
4. Colman DR, Lindsay MR, Amenabar MJ, Boyd ES. The intersection of geology, geochemistry, and microbiology in continental hydrothermal systems. *Astrobiology.* 2019;19:1505-22.
5. Peacock JP, Cole JK, Murugapiran SK, Dodsworth JA, Fisher JC, Moser DP, et al. Pyrosequencing reveals high-temperature cellulolytic microbial consortia in Great Boiling Spring after in situ lignocellulose enrichment. *PLoS One.* 2013;8:e59927.
6. Hua ZS, Wang YL, Evans PN, Qu YN, Goh KM, Rao YZ, et al. Insights into the ecological roles and evolution of methyl-coenzyme M reductase-containing hot spring Archaea. *Nat Commun.* 2019;10:4574.
7. Wang J, Qu Y-N, Evans PN, Guo Q, Zhou F, Nie M, et al. Evidence for nontraditional *mcr*-containing archaea contributing to biological methanogenesis in geothermal springs. *Science Advances.* 2023;9:eadg6004.
8. Klenk H-P, Clayton RA, Tomb J-F, White O, Nelson KE, Ketchum KA, et al. The complete genome sequence of the hyperthermophilic, sulphate-reducing archaeon *Archaeoglobus fulgidus*. *Nature.* 1997;390:364-70.
9. Slobodkina G, Allieux M, Merkel A, Cambon-Bonavita MA, Alain K, Jebbar M, et al. Physiological and genomic characterization of a hyperthermophilic archaeon *Archaeoglobus neptunius* sp. nov. isolated from a deep-sea hydrothermal vent warrants the reclassification of the genus *Archaeoglobus*. *Front Microbiol.* 2021;12:679245.
10. von Jan M, Lapidus A, Glavina Del Rio T, Copeland A, Tice H, Cheng J-F, et al. Complete genome sequence of *Archaeoglobus profundus* type strain (AV18T). *Stand Genomic Sci.* 2010;2:327-46.
11. Anderson I, Risso C, Holmes D, Lucas S, Copeland A, Lapidus A, et al. Complete genome sequence of *Ferroglobus placidus* AEDII12DO. *Stand Genomic Sci.* 2011;5:50-60.
12. Mardanov AV, Slododkina GB, Slobodkin AI, Beletsky AV, Gavrillov SN, Kublanov IV, et al. The *Geoglobus acetivorans* genome: Fe (III) reduction, acetate utilization, autotrophic growth, and degradation of aromatic compounds in a hyperthermophilic archaeon. *Appl Environ Microbiol.* 2015;81:1003-12.
13. Manzella MP, Holmes DE, Rocheleau JM, Chung A, Reguera G, Kashefi K. The complete genome sequence and emendation of the hyperthermophilic, obligate iron-reducing archaeon “*Geoglobus ahangari*” strain 234T. *Stand Genomic Sci.* 2015;10:77.

14. Stokke R, Hocking WP, Steinsbu BO, Steen IH. Complete genome sequence of the thermophilic and facultatively chemolithoautotrophic sulfate reducer *Archaeoglobus sulfaticallidus* strain PM70-1T. *Genome Announc.* 2013;1:e00406-13.
15. Boyd JA, Jungbluth SP, Leu AO, Evans PN, Woodcroft BJ, Chadwick GL, et al. Divergent methyl-coenzyme M reductase genes in a deep-subseafloor Archaeoglobi. *ISME J.* 2019;13:1269-79.
16. Mukherjee S, Seshadri R, Varghese NJ, Eloë-Fadrosch EA, Meier-Kolthoff JP, Göker M, et al. 1,003 reference genomes of bacterial and archaeal isolates expand coverage of the tree of life. *Nat Biotechnol.* 2017;35:676-83.
17. Buessecker S, Chadwick GL, Quan ME, Hedlund BP, Dodsworth JA, Dekas AE. Mcr-dependent methanogenesis in Archaeoglobaceae enriched from a terrestrial hot spring. *ISME J.* 2023;17:1649-59.
18. Apprill A, McNally S, Parsons R, Weber L. Minor revision to V4 region SSU rRNA 806R gene primer greatly increases detection of SAR11 bacterioplankton. *Aquat Microb Ecol.* 2015;75:129-37.
19. Bolyen E, Rideout JR, Dillon MR, Bokulich NA, Abnet CC, Al-Ghalith GA, et al. Reproducible, interactive, scalable and extensible microbiome data science using QIIME 2. *Nat Biotechnol.* 2019;37:852-7.
20. Martin M. Cutadapt removes adapter sequences from high-throughput sequencing reads. *EMBnetJ.* 2011;17:10-2.
21. Callahan BJ, McMurdie PJ, Rosen MJ, Han AW, Johnson AJ, Holmes SP. DADA2: High-resolution sample inference from Illumina amplicon data. *Nat Methods.* 2016;13:581-3.
22. Quast C, Pruesse E, Yilmaz P, Gerken J, Schweer T, Yarza P, et al. The SILVA ribosomal RNA gene database project: improved data processing and web-based tools. *Nucleic Acids Res.* 2012;41:D590-D6.
23. Davis NM, Proctor DM, Holmes SP, Relman DA, Callahan BJ. Simple statistical identification and removal of contaminant sequences in marker-gene and metagenomics data. *Microbiome.* 2018;6:226.
24. Aramaki T, Blanc-Mathieu R, Endo H, Ohkubo K, Kanehisa M, Goto S, et al. KofamKOALA: KEGG Ortholog assignment based on profile HMM and adaptive score threshold. *Bioinformatics.* 2020;36:2251-2.
25. Lu S, Wang J, Chitsaz F, Derbyshire MK, Geer RC, Gonzales NR, et al. CDD/SPARCLE: the conserved domain database in 2020. *Nucleic Acids Res.* 2020;48:D265-D8.
26. Sondergaard D, Pedersen CN, Greening C. HydDB: A web tool for hydrogenase classification and analysis. *Sci Rep.* 2016;6:34212.
27. Blum M, Chang H-Y, Chuguransky S, Grego T, Kandasaamy S, Mitchell A, et al. The InterPro protein families and domains database: 20 years on. *Nucleic Acids Res.* 2021;49:D344-D54.
28. Neukirchen S, Sousa FL. DiSCo: a sequence-based type-specific predictor of Dsr-dependent dissimilatory sulphur metabolism in microbial data. *Microb Genom.* 2021;7(7).

29. Neukirchen S, Sousa FL. DiSCo: a sequence-based type-specific predictor of Dsr-dependent dissimilatory sulphur metabolism in microbial data. *Microb Genom.* 2021;7:000603.
30. Price MN, Dehal PS, Arkin AP. FastTree 2--approximately maximum-likelihood trees for large alignments. *PLoS One.* 2010;5:e9490.
31. Jay ZJ, Beam JP, Dlakic M, Rusch DB, Kozubal MA, Inskeep WP. Marsarchaeota are an aerobic archaeal lineage abundant in geothermal iron oxide microbial mats. *Nat Microbiol.* 2018;3:732-40.
32. Zaremba-Niedzwiedzka K, Caceres EF, Saw JH, Backstrom D, Juzokaite L, Vancaester E, et al. Asgard archaea illuminate the origin of eukaryotic cellular complexity. *Nature.* 2017;541:353-8.
33. Edgar RC. MUSCLE: multiple sequence alignment with high accuracy and high throughput. *Nucleic Acids Res.* 2004;32:1792-7.
34. Katoh K, Standley DM. MAFFT multiple sequence alignment software version 7: improvements in performance and usability. *Mol Biol Evol.* 2013;30:772-80.
35. Capella-Gutiérrez S, Silla-Martínez JM, Gabaldón T. trimAl: a tool for automated alignment trimming in large-scale phylogenetic analyses. *Bioinformatics.* 2009;25:1972-3.
36. Minh BQ, Schmidt HA, Chernomor O, Schrempf D, Woodhams MD, von Haeseler A, et al. IQ-TREE 2: new models and efficient methods for phylogenetic inference in the genomic era. *Mol Biol Evol.* 2020;37:1530-4.
37. Rusch A, Amend JP. Order-specific 16S rRNA-targeted oligonucleotide probes for (hyper) thermophilic archaea and bacteria. *Extremophiles.* 2004;8:357-66.
38. Stahl DA. Development and application of nucleic acid probes in bacterial systematics. In: Stackebrandt E, Goodfellow, M, editor. *Nucleic acid techniques in bacterial systematics.* Chichester, UK: John Wiley & Sons Ltd; 1991. p. 205-49.
39. Pernthaler A, Pernthaler J, Amann R. Fluorescence in situ hybridization and catalyzed reporter deposition for the identification of marine bacteria. *Appl Environ Microbiol.* 2002;68:3094-101.
40. Schaible GA, Kohtz AJ, Cliff J, Hatzenpichler R. Correlative SIP-FISH-Raman-SEM-NanoSIMS links identity, morphology, biochemistry, and physiology of environmental microbes. *ISME Commun.* 2022;2:52.
41. Vaughan RG, Heasler HP, Jaworowski C, Lowenstern JB, Keszthelyi LP. Provisional maps of thermal areas in Yellowstone National Park based on satellite thermal infrared imaging and field observations. Reston, VA: U.S. Geological Survey; 2014.